West African Monsoon observed with ground-based GPS receivers during African Monsoon Multidisciplinary Analysis (AMMA)

Olivier Bock, Marie-Noëlle Bouin, E. Doerflinger, P. Collard, F. Masson, Rémi Meynadier, Samuel Nahmani, M. Koité, K. Gaptia Lawan Balawan, Francis Didé, et al.

West African Monsoon observed with ground-based GPS receivers during African Monsoon Multidisciplinary Analysis (AMMA)

O. Bock,[1,2] M. N. Bouin,[1] E. Doerflinger,[3] P. Collard,[3] F. Masson,[4] R. Meynadier,[2] S. Nahmani,[1] M. Koité,[5] K. Gaptia Lawan Balawan,[6] F. Didé,[7] D. Ouedraogo,[8] S. Pokperlaar,[9] J.-B. Ngamini,[10] J. P. Lafore,[11] S. Janicot,[12] F. Guichard,[11,13] and M. Nuret[11]

Received 25 April 2008; revised 24 July 2008; accepted 20 August 2008; published 5 November 2008.

[1] A ground-based GPS network has been established over West Africa in the framework of African Monsoon Multidisciplinary Analysis (AMMA) in tight cooperation between French and African institutes. The experimental setup is described and preliminary highlights are given for different applications using these data. Precipitable water vapor (PWV) estimates from GPS are used for evaluating numerical weather prediction (NWP) models and radiosonde humidity data. Systematic tendency errors in model forecasts are evidenced. Correlated biases in NWP model analyses and radiosonde data are evidenced also, which emphasize the importance of radiosonde humidity data in this region. PWV and precipitation are tightly correlated at seasonal and intraseasonal timescales. Almost no precipitation occurs when PWV is smaller than 30 kg m^{-2}. This limit in PWV also coincides well with the location of the intertropical discontinuity. Five distinct phases in the monsoon season are determined from the GPS PWV, which correspond either to transition or stationary periods of the West African Monsoon system. They may serve as a basis for characterizing interannual variability. Significant oscillations in PWV are observed with 10- to 15-day and 15- to 20-day periods, which suggest a strong impact of atmospheric circulation on moisture and precipitation. The presence of a diurnal cycle oscillation in PWV with marked seasonal evolutions is found. This oscillation involves namely different phasing of moisture fluxes in different layers implying the low-level jet, the return flow, and the African Easterly Jet. The broad range of timescales observed with the GPS systems shows a high potential for investigating many atmospheric processes of the West African Monsoon.

Citation: Bock, O., et al. (2008), West African Monsoon observed with ground-based GPS receivers during African Monsoon Multidisciplinary Analysis (AMMA), *J. Geophys. Res.*, *113*, D21105, doi:10.1029/2008JD010327.

1. Introduction

[2] The West African Monsoon (WAM) system has been the subject of intensive and growing research efforts during the last decades. This interest was primarily motivated by the need to understand the mechanisms responsible for the severe droughts that West Africa has undergone since the 1970s and increased interannual variability in rainfall [*Le Barbé et al.*, 2002]. Rainfall abundance is indeed of crucial importance in vulnerable regions such as the Sahel. The impact of interannual rainfall variability is increasing as the population and demand for water resources are quickly growing and are accompanied in some places by increased changes in land use and water pollution. Past studies have given evidence that the WAM system results from the interplay of various processes, involving multiple scale interactions between the ocean, land surface and vegetation, and the atmosphere. The African Monsoon Multidisciplinary Analysis program (AMMA), has been setup to improve our understanding of the WAM system as well as the environmental and socioeconomic impacts [*Redelsperger et al.*, 2006]. This program relies on embedded field experi-

[1]IGN, LAREG, Marne-la-Vallée, France.
[2]Service d'Aéronomie, Université Pierre et Marie Curie, UMR7620, CNRS, Paris, France.
[3]Géosciences Montpellier, Université Montpellier II, UMR5243, CNRS, Montpellier, France.
[4]IPGS, Université Louis Pasteur, UMR7516, CNRS, Strasbourg, France.
[5]Direction Nationale de la Météorologie, Bamako, Mali.
[6]Direction de la Météorologie du Niger, Niamey, Niger.
[7]Direction Nationale de la Météorologie, Cotonou, Benin.
[8]ASECNA, Ouagadougou, Burkina-Faso.
[9]Ghana Meteorological Agency, Tamale, Ghana.
[10]ASECNA, Dakar, Senegal.
[11]CNRM, Meteo-France, Toulouse, France.
[12]LOCEAN, Université Pierre et Marie Curie, UMR7159, CNRS, Paris, France.
[13]GAME, URA1357, CNRS, Toulouse, France.

0148-0227/08/2008JD010327

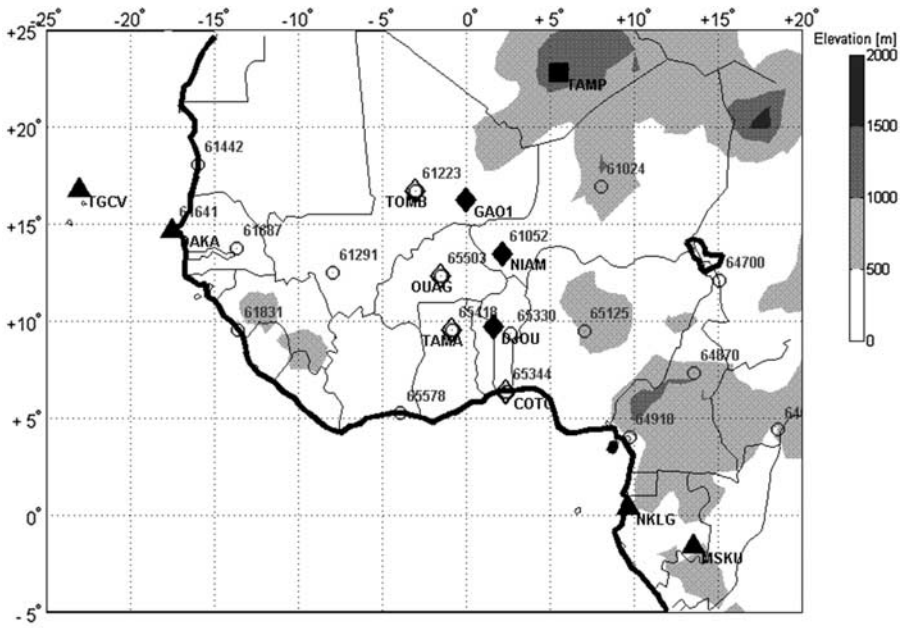

Figure 1. View of GPS receivers and radiosonde stations operating during the AMMA-EOP (2005–2007) and SOP (2006) campaigns. The GPS sites are indicated as symbols with four-letter identifications and the radiosonde sites are indicated as circles with five-digit identifications. The GPS sites comprise: four IGS sites (solid triangles), three AMMA-EOP sites (solid diamonds), three AMMA-SOP sites (open diamonds), TAMP (square), an Algerian permanent station, and COTO (open diamond), an AMMA test station installed in 2005. Grey shading shows topography (see axis on the right).

ments aiming at documenting the different components and scales (T. Lebel et al., The AMMA field campaigns: Multiscale and multidisciplinary observations in the West African region, submitted to *Annales Geophysicae*, 2008). This unprecedented effort should lead to major improvements in our understanding of the WAM system and its interactions with the global climate [*D'Orgeval et al.*, 2005] and in our capability to simulate this system, including better weather and seasonal forecasts.

[3] As part of the AMMA instrumental setup, we established a network of six ground-based Global Positioning System (GPS) receivers over West Africa. The GPS technique has shown to provide accurate estimates of precipitable water vapor (PWV), with high temporal resolution (typically hourly) and all-weather capability [*Bock et al.*, 2007b]. Atmospheric humidity is indeed a key ingredient of the water cycle and related processes such as convection and precipitation, which are of primary importance in the WAM system. A few previous studies have illustrated the large seasonal cycle in PWV that is associated with monsoon systems [*Takiguchi et al.*, 2000; *Singh et al.*, 2004; *Li and Chen*, 2005; *Bock et al.*, 2007a, *Kursinski et al.*, 2008].

[4] The GPS receivers operated during AMMA have been deployed along the meridian climatic gradient between the Guinean coast and the Sahara (Figure 1). The continuous operations of these receivers allow monitoring the total atmospheric humidity in different climatic areas and investigating atmospheric processes in a broad range of timescales, from subdiurnal to seasonal cycle. For example, a crucial aspect is the seasonal evolution of the rainbelt over the region which has been shown to be discontinuous and consisting in a succession of active phases and pauses [*Sultan and Janicot*, 2003; *Lebel et al.*, 2003; *Louvet et al.*, 2003]. The mechanisms intervening in this process are still under discussion [*Ramel et al.*, 2006], but their relation with atmospheric moisture fluxes may be important and show large interannual variability [*Fontaine et al.*, 2003]. At shorter timescales, intraseasonal variability with periodicities of 15 and 40 days [*Sultan et al.*, 2003; *Matthews*, 2004; *Mounier et al.*, 2007] and synoptic variability in rainfall and convection at timescales smaller than 10 days [*Redelsperger et al.*, 2002] are especially important as they modulate strongly the seasonal rainfall. The origin and role played by moist and dry air in these processes in the WAM system may be especially important [*Roca et al.*, 2005]. A significant correlation between atmospheric dynamics and PWV has been observed in the region of Dakar (15°N, 17°W) at intraseasonal to synoptic timescales [*Bock et al.*, 2007a]. With the AMMA GPS receivers, it is now possible to investigate whether such a correlation is also evident over central Sahel. Another fundamental timescale of the WAM system is the diurnal cycle. During the wet season, a strong diurnal cycle in convection sets in over continental West Africa [*Yang and Slingo*, 2001; *Mohr*, 2004]. The high-resolution GPS data help documenting the diurnal cycle in PWV and investigating the processes linking lower tropospheric moisture and precipitation [*Bock et al.*, 2007a; *Kursinski et al.*, 2008]. The GPS data are also useful for the validation of humidity observations from radiosondes and satellites, as well as from NWP model analyses and forecasts [*Hagemann et al.*, 2003; *Bock et al.*, 2007b; *Wang and Zhang*, 2008].

[5] The aim of this paper is to introduce the GPS network established during AMMA and to provide some preliminary

Table 1. Location and Coordinates of GPS Stations in IGS00 Reference Frame and Altitudes Given Above Mean Sea Level[a]

Location, Country	Identification	Latitude (°N)	Longitude (°E)	Ellipsis height (m)	Altitude (m)	Receiver Antenna Mount	Meteorological Sensor	Data Transfer Link	Operations	Comments
Cotonou, Benin	COTO	6.4	2.4	35	12	Ashtech DMCR Roof	N/A	N/A	20 Dec 2004 to Aug 2005	
Djougou, Benin	DJO1	9.7	1.7	460	436	Ashtech DMCR Tripod	N/A	N/A	05 June 2005 to 21 July 2005	
	DJOU	9.7	1.7	460	436	Trimble Zephyr Pillar	Vaisala, PTU200	Inmarsat	24 Aug 2005 to present	Radome removed 04 April 2006
Niamey, Niger	NIAM	13.5	2.2	246	223	Ashtech DMCR Pillar	N/A	N/A	05 June 2005 to 25 Aug 2005	
	NIAM	13.5	2.2	246	223	Trimble Zephyr Pillar	Vaisala, PTU200	VSAT	26 Aug 2005 to present	Radome removed 07 April 2006
Gao, Mali	GAO0	16.3	0.0	297	272	Ashtech DMCR Roof	N/A	N/A	11 June 2005 to 28 Aug 2005	
	GAO1	16.3	0.0	285	260	Trimble Zephyr Pillar	Vaisala, PTU200	Inmarsat	29 Aug 2005 to present	Radome removed 19 April 2006
Ouagadougou, Burkina-Faso	OUAG	12.4	−1.5	331	305	Trimble Zephyr Pillar	Vaisala, PTU200	GSM	30 May 2006 to present	
Tamale, Ghana	TAMA	9.6	−0.9	195	170	Trimble Zephyr Pillar	Vaisala, PTU200	GSM	23 April 2006 to present	
Tombouctou, Mali	TOMB	16.7	−3.0	292	263	Trimble Zephyr Pillar	Vaisala, PTU200	GSM	17 April 2006 to present	PTU200 installed 19 June 2006

[a]Description of equipment: Ashtech receivers are Z-Xtreme, Trimble receivers are NetRS. The Trimble Zephyr antennas were initially installed with radomes. The radomes were removed in April 2006. N/A denotes not available.

highlights of the potential of these data. In section 2, we describe the instrumental setup. In section 3 we describe different data processing procedures (both near-real time and postprocessing) and investigate their accuracy. In section 4 we present results of NWP model evaluation using both near-real time GPS PWV estimates (as delivered during the AMMA field experiment in 2006) and precise postprocessed GPS solutions. We show also evidence of humidity biases in the radiosonde data collected during the experiment, at six collocated GPS and radiosonde sites, which have a detrimental impact on the quality of NWP model analyses. In section 5 we focus on the description of the seasonal evolution of atmospheric humidity and precipitation for years 2005 and 2006. We show that PWV is a good diagnostic parameter describing the large-scale evolution of atmospheric moisture linked to the WAM. We identify several different periods between the establishment and retreat of the monsoon, which depend on the latitude of the site. We also discuss the seasonal evolution of the diurnal cycle in PWV and related atmospheric processes. Section 6 concludes and draws perspectives.

2. GPS Experimental Setup

[6] The location of the GPS receivers installed in the framework of AMMA is shown in Figure 1, along with the GPS receivers pertaining to the International GNSS Service (IGS), and the radiosonde (RS) network over West Africa as operational in summer 2006. Three of the GPS receivers have been installed in June 2005: Djougou (Benin), Niamey (Niger), and Gao (Mali). This transect is aiming at monitoring the PWV evolution along the climatological gradient of West Africa during the Enhanced Observing Period (EOP; 2005 to 2007 and possibly beyond) of AMMA, i.e., with emphasis on interannual variability. In April-May 2006, another transect of three GPS receivers has been installed at Tamale (Ghana), Ouagadougou (Burkina-Faso), and Tombouctou (Mali). This second GPS transect completes the first one in providing a more two-dimensional view of the PWV distribution in the WAM domain, though its zonal extension is limited. This enhanced GPS network targets features such as propagative waves and applications such as the computation of fine-scale water budgets from observational data (combining GPS and RS data) and/or from NWP models (with GPS data eventually assimilated). The second GPS transect was planned to operate only during the Special Observing Period (SOP; June-September 2006), but thanks to the operational facilities provided by the hosting institutes, these receivers are still operating in 2008.

[7] The geographic coordinates and details about the instruments, site logistics and operation dates are given in Table 1. During a preliminary test period, between December 2004 and August 2005, a GPS station from the French mobile GPS facility of Institut National des Sciences de l'Univers (INSU)/CNRS has been installed at the IRD center in Cotonou, Benin. In June 2005, three other GPS stations from INSU/CNRS have been installed in Djougou, Niamey and Gao, on the EOP transect. These stations were composed of high-quality geodetic receivers (Ashtech, X-treme) and antennas (Dorne Margolin Choke Ring; DMCR). The final EOP systems were installed in August 2005 and the GPS

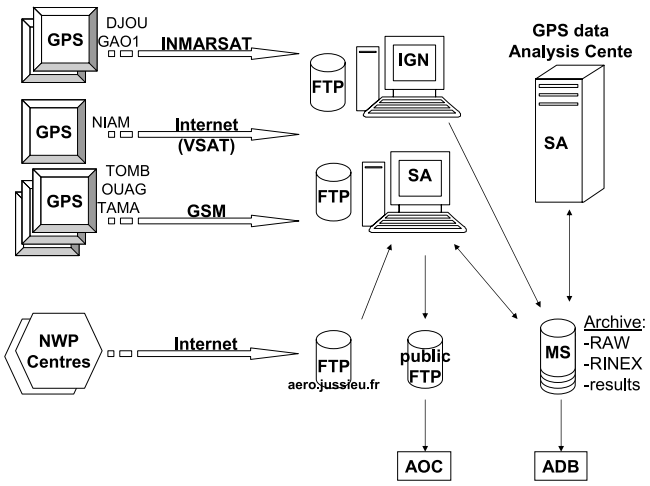

Figure 2. Schematics of data flow during the AMMA SOP. Data are collected at IGN and Service d'Aéronomie (SA), processed at SA, and a near-real-time NWP model verification product is made available to the AMMA operations center (AOC). The precise solutions are archived at SA and made available to the AMMA database (ADB).

station at Cotonou was dismounted. These systems were funded by INSU/CNRS in the frame of the French AMMA program, and are planned for long-term operations. They are composed of high-quality geodetic receivers (Trimble, NetRS) and antennas (Trimble, Zephyr), meteorological stations (Vaisala, PTU200) and different kinds of data transmission systems. The SOP systems installed in April-May 2006 are similar to the EOP systems in order to guarantee high consistency. All the antennas are mounted on reinforced concrete pillars of 1-m height above ground, with a massive basement ($\sim$1 m^3 of concrete) of 1 m depth under the ground surface. This monumentation should guarantee stable measurements (with submillimeter vertical accuracy). Radomes were initially mounted on the antennas, but were later removed (April 2006) in order to prevent from excessive heating of the antennas.

[8] The data flow is depicted in Figure 2. Data transmission is a crucial issue for operational and/or long-term applications. Inmarsat modems have been installed at Djougou and Gao stations in order to transmit raw data files daily to the analysis center at Service d'Aéronomie/CNRS in Paris, France. Cellphone (GSM) modems are used at SOP sites, which allow connecting to the station and checking operations but not transferring the data files (owing to limitations in data transmission rate). At Niamey, a local radio link makes the bridge between the GPS station at the airport and the satellite link shared between African Centre of Meteorological Application for Development (ACMAD), Direction Nationale de la Météorologie (DMN), and Agence pour la Sécurité de la Navigation aérienne en Afrique et à Madagascar (ASECNA). This link permits to transmit data several times a day, which allowed us to produce GPS Zenith Tropospheric Delay (ZTD) and PWV solutions in near-real time during the SOP. These solutions were used during the SOP for assessing forecasts from several NWP models. The comparisons were delivered in real time to the AMMA Operational Centres (AOCs) in Niamey and Toulouse http://aoc.amma-international.org/index.en.php).

3. GPS ZTD and PWV Retrieval Procedures

[9] The GPS data were processed using the GAMIT scientific software [*King and Bock*, 2005], within a regional network including all the available AMMA stations and permanent GPS stations in the Northern part of Africa, as well as several good quality IGS stations in southern Europe, Middle East, Indian Ocean and Atlantic Ocean. The number of stations was held smaller than 25, in order to keep reasonable processing time, and larger than 15, to ensure moderate intersite distances and good spatial coverage. Owing to the scarcity of IGS stations in West Africa (see Figure 1), the mean intersite distance for AMMA stations was about 4500 km (the smallest was 400 km). The GPS data are processed in two different ways. First, an operational procedure is running automatically and producing ZTD solutions with different delays and innovation periods as reported in Table 2. Second, a reprocessing is performed when significant improvements are available (new software versions) and validated. The near-real time/operational (''NRT/oper'') procedure contains only the AMMA station at Niamey (the only station where data could be transmitted reliably every 3 h) during the SOP 2006. The ''rapid/oper'' procedure contains the GPS stations at Niamey, Djougou and Gao for which daily data transfer was more or less achieved. The ''precise/oper'' procedure contains eventually all AMMA stations (it is repeated each time new data arrive from these stations). The rapid and precise versions were useful for intercomparison and rapid verification purposes. Therefore, the processing strategies for the three operational versions were kept as similar as possible throughout the EOP and used a

Table 2. Difference in Processing Strategies[a]

	Latency	Start Time of Session	Duration of Session	Type of Orbit	Number of Stations	Tropospheric Model
NRT/oper	1 h 30 from last measurement	0000, 0300... 2100 UTC	12 h	IGU predicted	16	NMF/STP
Rapid/oper	4 h from last measurement	0000 UTC	24 h	IGU computed	16	NMF/STP
Precise/oper	13–15 days	0000 UTC	24 h	IGS final	25	NMF/STP
Precise/repro	13–15 days	0000/1200 UTC	24 h each (sliding window)	IGS final	25	GMF/GPT

[a]Near-real time (NRT), rapid and precise during 2005 and 2006 operations (oper) and reprocessed (repro) using a more recent version of the software. See text for details on the tropospheric models other processing parameters.

fixed software version (GAMIT v10.21). Only recently have all the data been reprocessed using a more recent version of the software (GAMIT v10.32) which includes improved tropospheric modeling capabilities and IGS products. This version (''precise/repro'') is used in the present study for verifying a posteriori the operational products. It is also this version that is used in the following sections focusing on scientific applications.

[10] The common processing parameters for the operational procedures are the following. The a priori dry and wet components of the tropospheric delay were calculated using *Saastamoinen*'s [1973] model and standard temperature and pressure model (P = 1013.25 hPa, T = 20°C and RH = 50% at sea level, referred to as STP50). Dry and wet mapping functions from *Niell* [1996] were applied to the respective a priori delays computed with *Saastamoinen*'s [1973] model and STP50, while the wet mapping function only was used for estimating the residual delay from the observations. The residual delay parameters were estimated every hour as nodes of a piecewise linear function determined from a first-order Gauss-Markov process, with constraints from a priori values of 0.5 m, point-to-point variation constraints of 0.02 m $h^{-1/2}$ and a correlation time of 100 h. The ZTD estimates were reconstructed as the sum of the a priori dry and wet components and the estimated residual delay. One set of tropospheric delay gradient parameters was estimated per session, whatever the session length. The cutoff elevation angle was set to 7° and a residual-dependent weighting of the observations was used. The IGS orbits were kept fixed, a priori station positions from IGS00 (R. Ferland, IGSMail 4748, 4758 and 4666, from 2003, available at http://igscb.jpl.nasa.gov/mail/igsmail/2003/maillist.html) were constrained with 50 cm a priori standard deviations, ocean tide loading effects were corrected at the observation level using the FES2004 model [*Lyard et al.*, 2006], solid Earth and polar tides were corrected following the IERS 2003 conventions, and absolute receiver and satellite antenna phase center variation models were used. We did not correct for atmospheric loading effects at the observation level as recommended by *Ray et al.* [2007]. The NRT/oper processing used the predicted part of the IGS ultra rapid (IGU) orbits. The session length was set to 12 h to get a sufficient number of simultaneous observations within the IGS NRT network (between 13 and 18 stations selected), and mitigate biases related to the orbit errors. The ''rapid/oper'' processing used the computed part of the IGU orbits, which is more accurate. Finally, ''precise/oper'' processing used the IGS final orbits with ultimate precision (2 to 3 cm) available 15 to 20 days after measurement.

[11] For the data reprocessing we used the more recent GMF mapping functions [*Boehm et al.*, 2006b] and GPT climatology [*Boehm et al.*, 2007] which were both derived from ECMWF 40-year reanalysis. The choice of this strategy rather than the more elaborate VMF1 mapping functions and gridded ZHD product [*Boehm et al.*, 2006a] was faster computation for the GPS data reprocessing. We evaluated the difference in ZTD estimates between these two strategies for two months. The differences remained very small both in terms of bias and standard deviation (<1 mm ZTD or <0.16 kg m^{-2} PWV). However, some improvement can be expected compared to the precise/oper solution according to *Tregoning and Herring* [2006] and *Boehm et al.* [2006a]. For the reprocessing we also used a sliding window technique [e.g., *Walpersdorf et al.*, 2007] in order to avoid edge effects (see discussion below). In this case, we processed the data in two 24-h sessions, one starting at 0000 UTC and one at 1200 UTC, from which the central 12 h were extracted as the final solutions. However, we did not account for atmospheric pressure loading effects [*Tregoning and van Dam*, 2005]. The nontidal vertical displacement is actually adjusted in the station coordinate estimates (hence not affecting ZTD estimates). On the other hand, the tidal components, when not modeled at the observation level, map directly into ZTD biases. But the amplitude of these components are so small over the AMMA area (1 and 1.1 mm, for diurnal and semidiurnal tides, respectively, estimated using the model from *Petrov and Boy* [2004] provided by the Goddard VLBI group at http://gemini.gsfc.nasa.gov/aplo) that their impact on ZTD can be neglected (ZTD error <0.3 mm and PWV error <0.05 kg m^{-2}).

[12] The conversion of GPS ZTD into PWV (hereafter, PWV_{GPS}) is performed in two steps [*Bevis et al.*, 1994]. First, the contribution of hydrostatic part of the air, referred to as zenith hydrostatic delay (ZHD), is evaluated at the location and time of the GPS observations and subtracted from ZTD. The calculation of ZHD is obtained from surface pressure observations, P_{surf}, using the formula of *Saastamoinen* [1973]: $ZHD = 2.279$ [mm hPa^{-1}] $\times$ P_{surf} [hPa]/f(φ_{sta}, h_{sta}), where f(φ_{sta}, h_{sta}) is a correction of the mean gravity, depending on the latitude, φ_{sta}, and altitude, h_{sta}, of the station. Second, the remainder is converted into PWV using a conversion factor $\kappa(T_m)$: $PWV_{GPS} = \kappa(T_m) \times (ZTD - ZHD)$. This factor depends on the mean temperature, T_m, in the column of atmosphere above the GPS antenna, and scales as $\sim$155 kg m^{-3} under standard atmospheric conditions. *Bevis et al.* [1994], modeled T_m as a linear function of temperature of air near the surface: $T_m = a \times T_{surf} + b$, with $a = 0.72$ and $b = 70.2$ K derived from a set of radiosonde data in the United States. These values have been used to convert the NRT and rapid ZTD solutions for the sake of simplicity. However, coefficients a and b are known to be season and latitude dependent [*Ross and Rosenfeld*, 1997]. Over West Africa, and in the tropics more generally, the correlation between T_m and T_{surf} is much smaller, as is the seasonal variation in a and b [*Ross and Rosenfeld*, 1997]. Using a linear model can induce errors of up to 1.5% PWV, i.e., 0.5–1 kg m^{-2} during the wet season. Because of these limitations and also the presence of an artificial diurnal cycle induced in T_m by T_{surf}, we now use T_m values provided by the Technical University of Vienna (http://mars.hg.tuwien.ac.at/~ecmwf1/). These values are computed from temperature and humidity profiles of the ECMWF operational analyses with a 6-h time resolution and 2° by 2.5° horizontal resolution globally. Figure 3 shows the typical diurnal variation of P_{surf}, ZHD, and T_m as modeled by *Bevis et al.* [1994] and computed from ECMWF profiles. A typical semidiurnal oscillation in surface pressure is observed [e.g., *Dai and Wang*, 1999], which induces an average variation in ZHD of 7 mm peak-to-peak. In order to eliminate properly this oscillation from ZTD, surface pressure must be sampled with sufficient time resolution. The mean amplitude of the T_m variation calculated from *Bevis et al.* [1994] model is about 6 K,

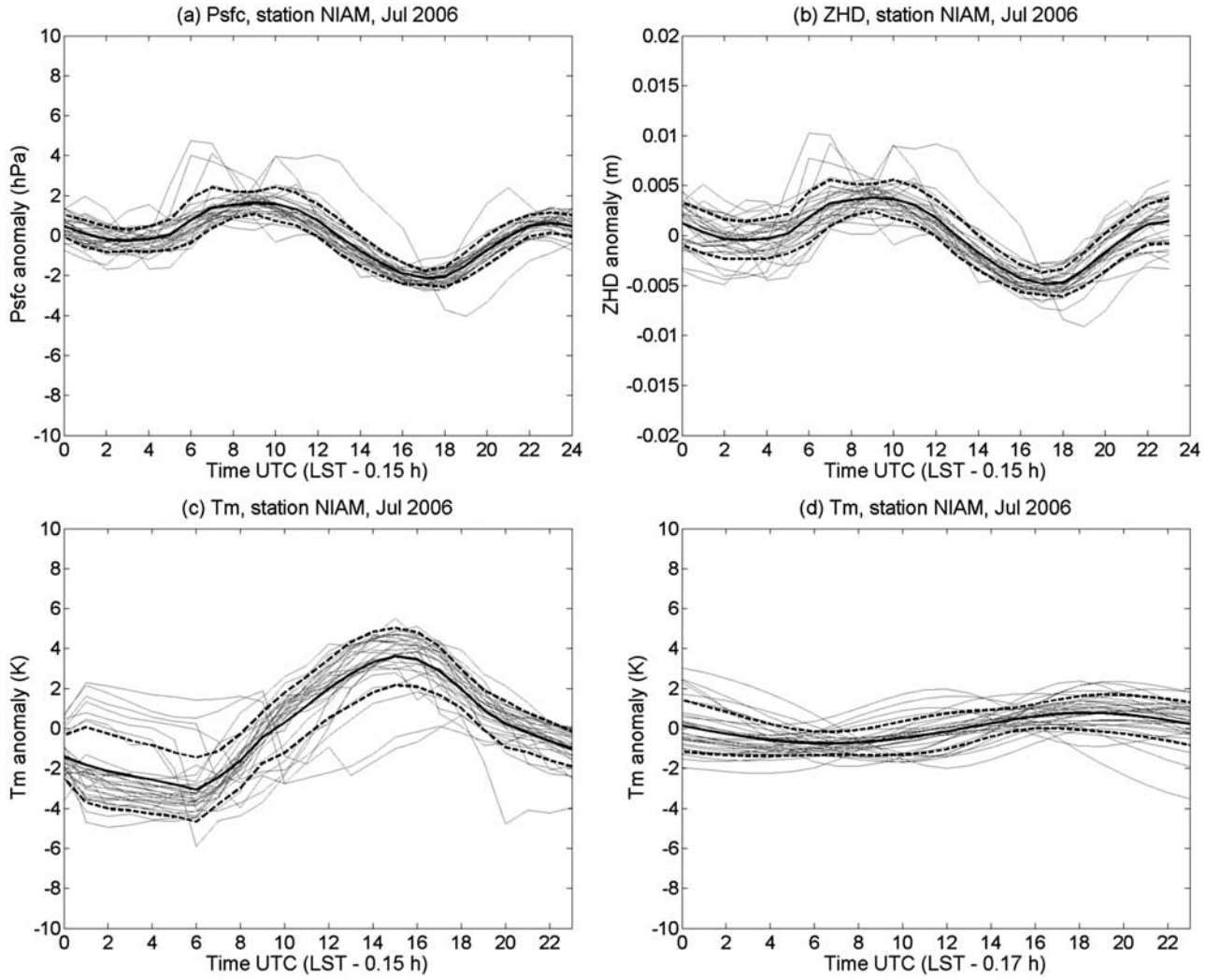

Figure 3. Diurnal evolution of parameters used for the conversion of GPS ZTD estimates into PWV at Niamey for July 2006: (a) observed surface pressure, (b) hydrostatic delay calculated from surface pressure, (c) mean temperature calculated from a linear relationship using observed 2-m temperature [*Bevis et al.*, 1994], and (d) mean temperature calculated from temperature and humidity profiles extracted from ECMWF model operational analysis. The light gray curves represent daily anomalies, and the bold black curves represent mean (solid curve) and ±1 standard deviation (dashed curves) around the mean.

peak-to-peak, which clearly overestimates the more accurate variation, calculated from ECWMF analyses (∼1 K). Using the former, a bias in PWV of 6 K/300 K = 2% may be introduced.

[13] The accuracy of GPS estimates can be assessed in different ways. The most common one is to compute the standard deviation of station coordinates (referred to as repeatability) expressed in a stable reference frame (in our case ITRF 2005 [*Altamimi et al.*, 2007]). In the case of our "precise/repro" GPS solution, the repeatability in the station coordinates of the AMMA GPS stations is fairly good (e.g., 2–4 mm on horizontal coordinates and 5.0 mm on the vertical for Niamey GPS station). A good repeatability in the vertical coordinate gives also good confidence into the accuracy of ZTD estimates at the same station; however, ZTD accuracy is more difficult to assess since this quantity is not stationary. Therefore, we use the "formal ZTD error" which is provided at the end of the GPS data analysis. This quantity is proportional to the postfit root mean square error (RMSE) of the GPS phase observations at each station. Figure 4 shows the diurnal evolution of the formal ZTD error for all four data processing solutions at station Niamey. It is seen that the accuracy is roughly constant throughout the day and at the level of 3 mm for the reprocessed data, while it exhibits higher values and marked edge effects for the other processings. The edge effects are due to the fact less observations are available in the first and last time bin of a given data window. The sliding window processing (Figure 4d) eliminates this effect, hence giving more confidence into the 0000 UTC ZTD estimates which are especially important for the radiosonde and NWP model verification discussed in section 4. Inspection of day-to-day variability in formal ZTD error (gray lines in Figure 4) at all the AMMA stations reveals that it is most of the time uncorrelated from one station to another. Hence, its origin is most likely due to variations in local error sources associated

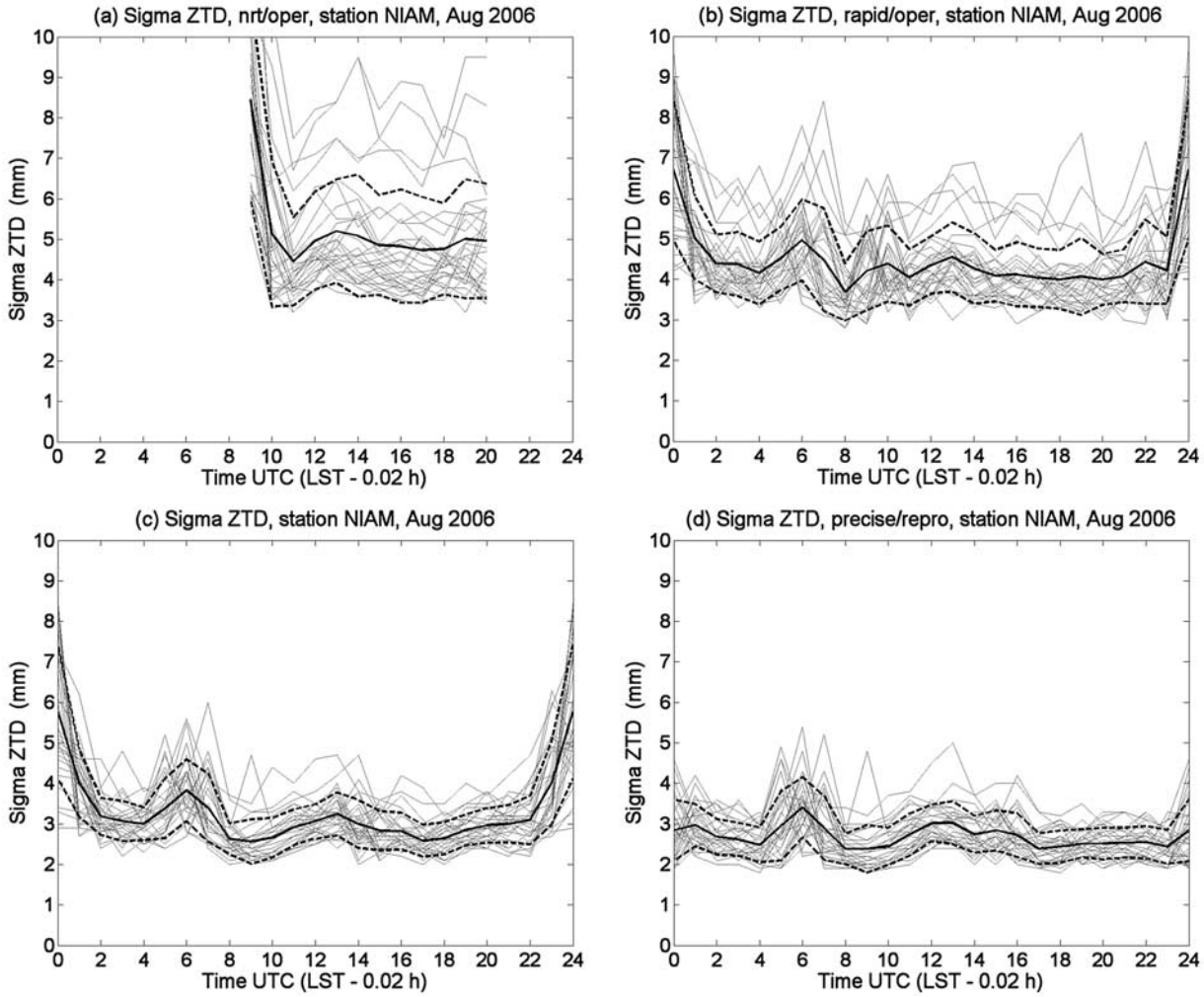

Figure 4. Diurnal evolution of formal accuracy in GPS ZTD estimates for (a) NRT/oper, (b) rapid/oper, (c) precise/oper, and (d) precise/repro. Light gray curves represent all days in the month (August 2006), and bold black curves represent mean (solid curve) and ±1 standard deviation (dashed curves) around the mean.

with each station (e.g., multipath, antenna phase center variations, tropospheric modeling error). In the case of the rapid and NRT solutions, variations are sometimes correlated between stations which are very likely due to orbit errors associated with the less accurate ultrarapid orbits (as reported by *Baltink et al.* [2002]). The inspection of formal ZTD error, ZTD (or PWV), outgoing long-wave radiation (OLR) and rain rate reveals frequent coincident variations in these quantities. This suggests some influence of meteorological conditions on ZTD accuracy.

[14] We now use our reprocessed solution for assessing the accuracy of the other processings. Table 3 presents the results of a comparison covering the period June-September 2006. The first two columns of Table 3 show the average parameters for the different processings (the precise/repro solution is repeated because of different samplings). It is seen that the temporal ZTD variability is properly and consistently represented by the different processings. The increase from the southern to the northern stations reveals an interesting climatic feature discussed later. The difference in formal ZTD errors reveals the impact of different processing strategies and IGS orbit accuracy. The mean ZTD values reveal also biases linked with these differences. On average, the two precise solutions show a difference of 2.6–4.1 mm ZTD (0.4–0.6 kg m^{-2} PWV) and a standard deviation of 4.2 mm ZTD (0.6 kg m^{-2} PWV) mainly due to changes in the tropospheric models. The rapid and NRT solutions show a bias of ~5 and ~7 mm ZTD (0.8–1.1 kg m^{-2} PWV), respectively, and a standard deviation of ~7 and ~15 mm, respectively, in ZTD (1.1–2.3 kg m^{-2} PWV) compared to "precise/repro." These results are consistent with, for example, those of *Ge et al.* [2002] and *Pacione and Vespe* [2003]. Figure 5 shows the differences between processings at Niamey for the month of August 2006. The differences increase slightly at the window edges as expected but the scatter remains <5 mm ZTD (<0.8 kg m^{-2} PWV) at one standard deviation.

[15] On the basis of the uncertainties assessed above and comparisons with independent PWV observational techniques [e.g., *Niell et al.*, 2001; *Haase et al.*, 2003; *Bock et al.*, 2007b], we can assume that the "precise" ZTD solutions have an accuracy of ~4 to 8 mm of ZTD (~0.6 to 1.3 kg m^{-2}

Table 3. Statistics of ZTD Solutions[a]

	Precise/Repro			Precise/Oper			Precise/Oper - Precise/Repro			
	Mean (mm)	Standard Deviation (mm)	Formal (mm)	Mean (mm)	Standard Deviation (mm)	Formal (mm)	Mean (mm)	Standard Deviation (mm)	Formal (mm)	Number of Points
Gao (16.3°N)	2459	54	3.0	2457	53	3.4	4.1	4.1	4.6	2774
Niamey (13.5°N)	2517	40	3.0	2520	41	3.4	2.6	4.2	4.6	2812
Djougou (9.7°N)	2480	27	2.8	2483	27	3.3	3.3	4.2	4.4	2901
	Precise/Repro			Rapid/Oper			Rapid/Oper - Precise/Repro			
	Mean (mm)	Standard Deviation (mm)	Formal (mm)	Mean (mm)	Standard Deviation (mm)	Formal (mm)	Mean (mm)	Standard Deviation (mm)	Formal (mm)	Number of Points
Gao	2455	54	3.0	2460	54	4.5	4.8	7.2	5.4	2449
Niamey	2518	40	3.0	2523	41	4.5	5.2	7.5	5.4	2634
Djougou	2480	27	2.8	2485	28	4.6	5.6	8.3	5.4	2813
	Precise/Repro			NRT/Oper			NRT/Oper - Precise/Repro			
	Mean (mm)	Standard Deviation (mm)	Formal (mm)	Mean (mm)	Standard Deviation (mm)	Formal (mm)	Mean (mm)	Standard Deviation (mm)	Formal (mm)	Number of Points
Niamey	2515	39	3.0	2522	41	6.2	7.2	14.8	6.9	2519

[a]From the operational processing (oper) and reprocessing (repro), as well as differences w.r.t. precise reprocessing at some AMMA GPS sites. For the NRT solution at Niamey, only the last 3 h are used. Data cover period June–September 2006.

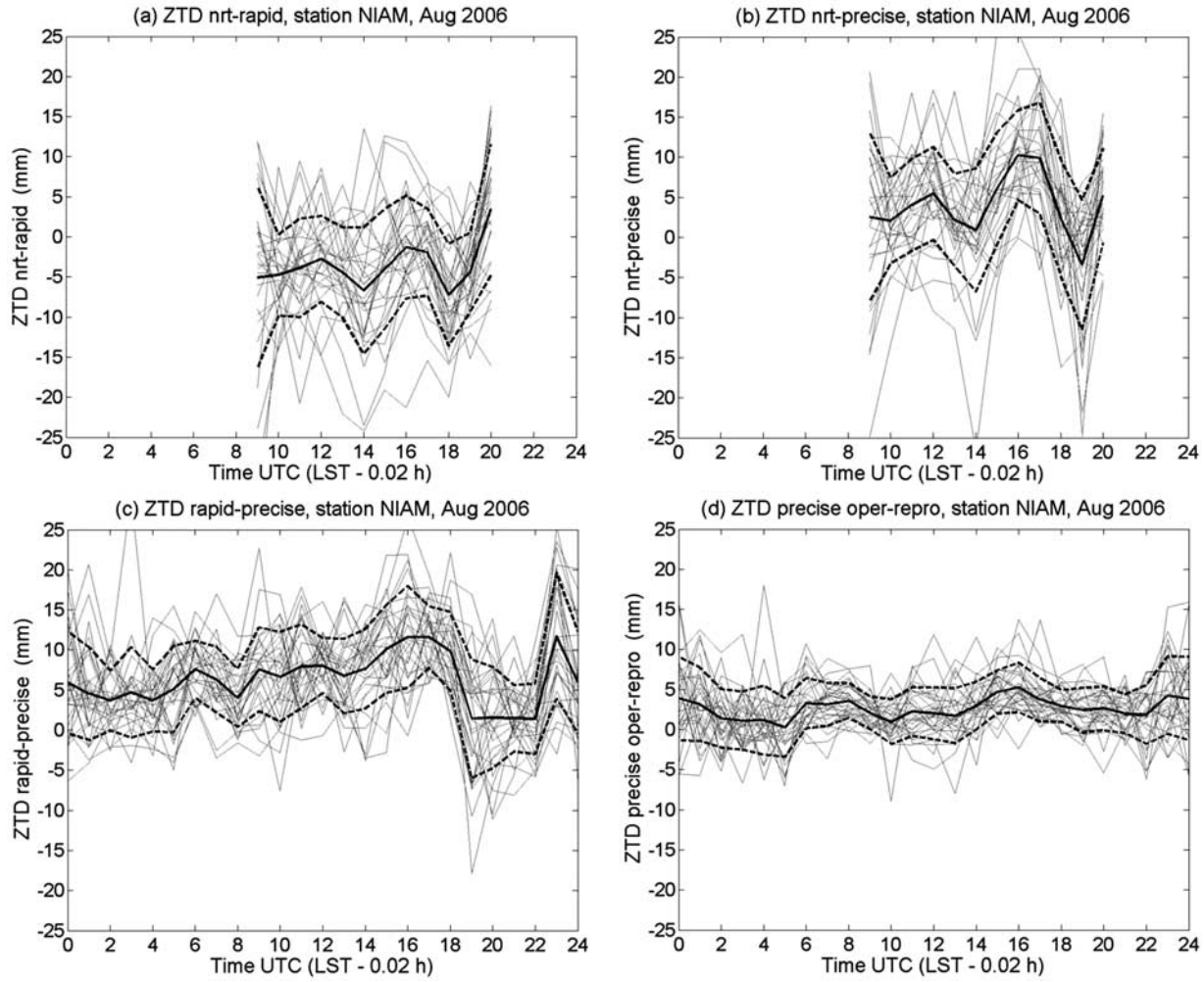

Figure 5. Diurnal evolution of differences in ZTD between GPS processing: (top left) NRT/oper – rapid/oper, (top right) NRT/oper – precise/repro, (bottom left) rapid/oper – precise/repro, and (bottom right) precise/oper – precise/repro. Light gray curves represent daily anomalies, and black curves represent mean and mean ±1 standard deviation. For the NRT solution, only the 0900–2000 UTC window is displayed.

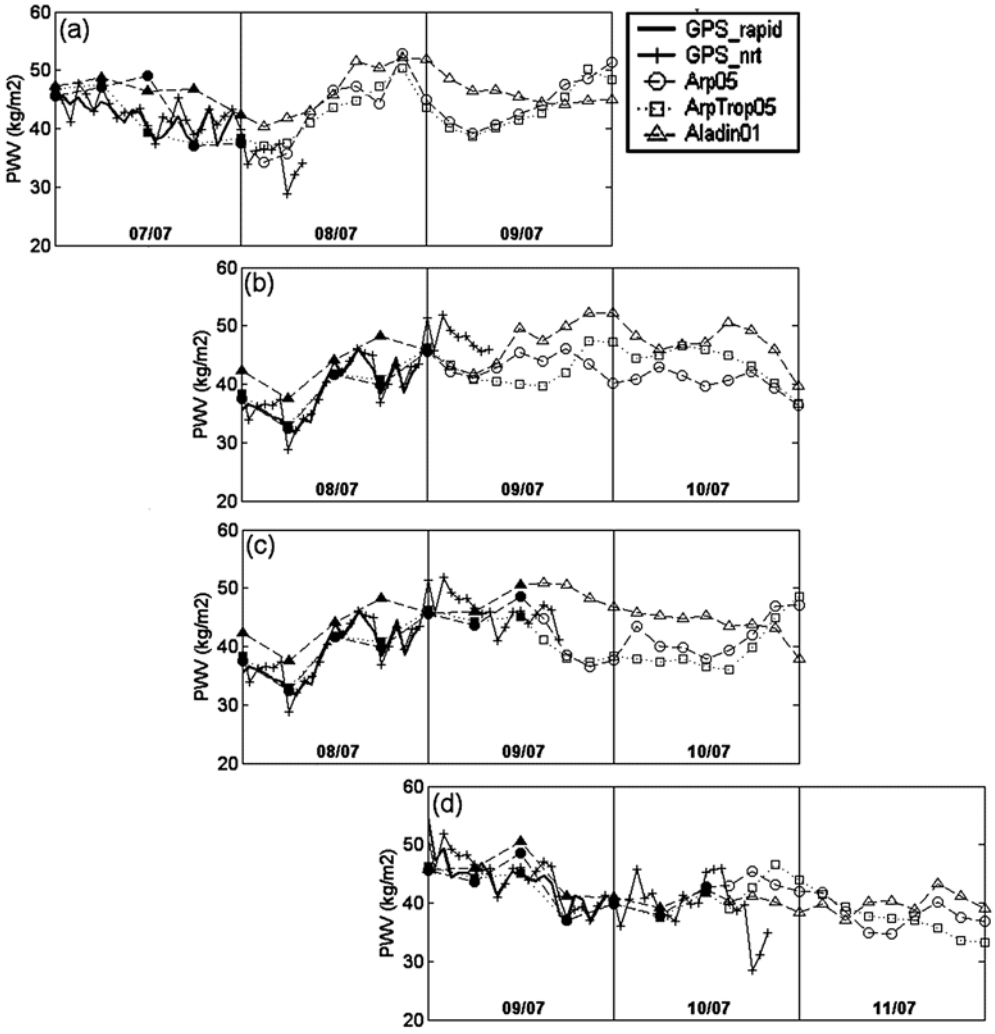

Figure 6. Verification of NWP PWV analyses (lines with solid symbols) and forecasts (lines with open symbols) with GPS PWV estimates from rapid (thick line) and NRT (line with plus signs) solutions at Niamey as produced in near-real time during the SOP (here a sample from July 2006). Each plot covers 3 days (the central day is the current one). The plots are updated as new NRT GPS estimates and/or model analyses and forecasts are available.

of PWV) while the "rapid" and NRT solutions have nearly twice and three times larger uncertainties, respectively. Only the comparison with a perfectly calibrated technique would allow estimating the bias in GPS PWV, but we believe that using the most recent processing strategy this bias uncertainty should be at the level of ± 3 mm ZTD (±0.5 kg m^{-2} IWV).

4. NWP Model and Radiosonde Data Verification With GPS

4.1. NWP Model Verification in Near-Real Time

[16] The NRT and rapid GPS solutions were used during the SOP for the evaluation of analyses and forecasts from Meteo-France NWP models: the global models ARPEGE and ARPEGE-Tropiques (at 0.5° horizontal resolution), and the limited area model ALADIN (at 0.1° horizontal resolution). The nearest model grid points were used here, which we believe should not induce significant representativeness differences compared to interpolated values thanks to the fine resolution of the models and knowing that PWV fields in these models have usually a broad spatial correlation (about a few hundred kilometers). Further details on the models are available at the AOC web site http://aoc.amma-international.org/index.en.php) or from M. Nuret et al. (Evaluation of METEO-FRANCE Numerical Weather Prediction models during AMMA 2006-SOP, 2007, http://www.cnrm.meteo.fr/aladin/newsletters/news32/news32.pdf) (hereinafter Nuret et al., online publication, 2007). Figure 6 shows an example of such evaluation, covering a moderate rain event (9 mm in Niamey) occurring during the night between 08 and 09 July 2006. This case has been selected to illustrate a typical series of analyses and successive corrections in the model forecasts associated with a spike in PWV followed by precipitation. Figure 6a shows the PWV contents valid at 1200 UTC on 08 July 2006, comprising: the NRT and rapid GPS estimates and NWP model analyzed values for the previous day (07 July), the NRT GPS estimates from 0000 to 0900 UTC on 08 July, and NWP model forecasted values every 3 hours up to +48 h (i.e.,

from 0300 UTC on 08 July to 0000 UTC on 10 July). The 3-day period covered by this plot is characterized by two spikes in the PWV forecasts (mainly from ARPEGE and ARPEGE-Tropiques) in the evenings of 08 and 09 July. The spikes reach 50 kg m^{-2} while at the beginning of the period, for example, at 0000 UTC of 08 July, the value is at a minimum of 35 kg m^{-2}. It is seen on subsequent plots that the first spike is properly predicted in amplitude, though too early by ~6 h (2100 instead of 0300 UTC). The GPS NRT estimates provide here valuable nowcasting information showing a minimum in PWV at 0600 UTC on 08 July and a starting increase later on. Figure 6b shows that the analyses from the different NWP models properly correct the forecasts for 08 July. The second spike, on the other hand, is mispredicted as seen from PWV observations showing a continuous decrease on 09 July below 40 kg m^{-2} (Figure 6d). This spike was forecasted since 0000 UTC 08 July (48 h ahead) but was only corrected from the following forecasts: 0000 UTC on 09 July for ARPEGE (Figure 6b) and 1200 UTC on 09 July from ARPEGE-Tropiques and ALADIN (Figure 6c). Figure 6d shows that the NWP analyses are recovering well the minimum in PWV on the end of 09 July. A similar but opposite behavior of the forecasts can also be seen for the end of 10 July. On Figure 6b, the +48 h forecasts predict an increase in PWV in the evening of that day while it is corrected in Figures 6c and 6d with the +36 h and +12 h forecasts, respectively.

[17] This short description reveals typical features of the West African Monsoon weather systems as observed from fixed points. The whole wet season exhibits a number of such spikes in PWV of a few-hour durations and amplitudes of 5 to 10 kg m^{-2} which are most of the time embedded in longer periods of increase/decrease of a few day durations (monsoon pulses, drying trends). Almost only the ground-based GPS receivers are capable of capturing these rapid variations. Most of them are associated with rainfall, at least at Niamey. It also emphasizes the difficulty the NWP models have to handle the atmospheric humidity and related processes (advection, convection, and precipitation) at sub-diurnal timescales. Most of the time, the PWV variations are not properly predicted, neither in amplitude, nor in time. The next section gives an overview of these problems at more sites and over the whole wet season.

4.2. NWP Model Verification With Precise GPS Data

[18] The precise reprocessed GPS solutions were used for a more accurate evaluation of NWP model analyses and forecasts. Here we describe only the results for the analyses and forecasts started at 0000 and 1200 UTC from ARPEGE. The results for the two other models were very similar. Some additional discussion of differences in precipitation forecasts between these models is given by Nuret et al. (online publication, 2007). Figure 7 shows the mean PWV from ARPEGE and GPS at the six AMMA GPS sites. Overall, GPS observations reveal a diurnal cycle in PWV with peak-to-peak amplitude between 1 kg m^{-2} (Niamey, Gao, and Tamale) and 2 kg m^{-2} (Djougou, Ouagadougou, and Tombouctou) further discussed in section 5.2. Overall, it is poorly reproduced in the model. Instead, the model shows trends toward smaller PWV values at southern stations and larger values at northern stations. The trends can be understood in terms of a northward migration of the Inter-Tropical Convergence Zone (ITCZ) with time in the ARPEGE forecasting system (Nuret et al., online publication, 2007). Superimposed to the trend, the diurnal cycle in PWV is quite properly phased at the southern sites but is out-phase at the northernmost ones. This may be linked to an incorrect phasing of convection [*Yang and Slingo*, 2001] and more broadly limitations in the parameterizations [*Betts and Jakob*, 2002] and assimilation systems [*Drusch and Viterbo*, 2007] used in such models for representing the hydrological cycle. We also observed a general increase in the standard deviation with forecast range (not shown). Another dramatic effect is seen for the 1200 UTC assimilation cycle where the analyses are systematically dryer than the forecasts and the GPS. This effect appears at all sites where radiosonde data are assimilated (i.e., all but Gao and Tombouctou at the time of the SOP). It is shown below that this feature is strongly correlated with dry biases diagnosed in the radiosonde humidity data.

4.3. Evaluation of Radiosonde Humidity Biases

[19] High-resolution radiosonde (RS) data archived on the AMMA database have been evaluated with precise reprocessed GPS PWV at six sites for the period June-September 2006 (Table 4). The RS stations used various types of sondes, some of which changed between 2005 and 2006. Unfortunately, sonde types have been mixed at some sites. While at most of the sites new sondes were used during the SOP (e.g., RS92 and MODEM), some went back to older sondes after the SOP (e.g., back to RS80 at Vaisala sites). Moreover, at Niamey RS80 and RS92 sondes were used alternatively during the intensive operations periods with 8 soundings per day. Figure 8 shows the biases at the four main synoptic hours; with indication of the types of sondes selected for the present comparison (i.e., the most frequently used sondes). Significant dry biases are seen at all sites at 1200 UTC, which reach 6–8 kg m^{-2} (15–25% of PWV) at sites using Vaisala RS80 sondes. The biases are smaller at Vaisala RS92 and MODEM sondes. Marked day/night differences are seen at all sites, which tend to be larger at Vaisala RS92 and MODEM sites than at Vaisala RS80 sites. Similar results have been obtained from other studies which attributed the dry bias to daytime solar radiation affecting both temperature and humidity measurements. The different behavior with sonde type was attributed to the fact that the humidity sensors of the RS80 sondes were protected by a cap while the other sensors were not [*Wang and Zhang*, 2008].

[20] The dry biases in the ARPEGE analyses (Figure 7) at 0000 and 1200 UTC are seen to match almost exactly the dry biases diagnosed here in the radiosonde data, at the four sites from which data were assimilated (Niamey, Parakou, Tamale, and Ouagadougou). This is consistent with previous investigations using ECMWF model analyses and first-guess minus RS observations statistics [*Bock et al.*, 2007b]. The large biases in the RS humidity data, and their impact in NWP model analyses, diagnosed with the help of the GPS PWV estimates, motivated the development of a correction scheme for the AMMA RS data [*Nuret et al.*, 2008]. This correction step is necessary before conducting further reanalysis experiments [*Agusti-Panareda and Beljaars*, 2008] and investigating a wide number of moist-processes related studies. The GPS PWV data may further help in

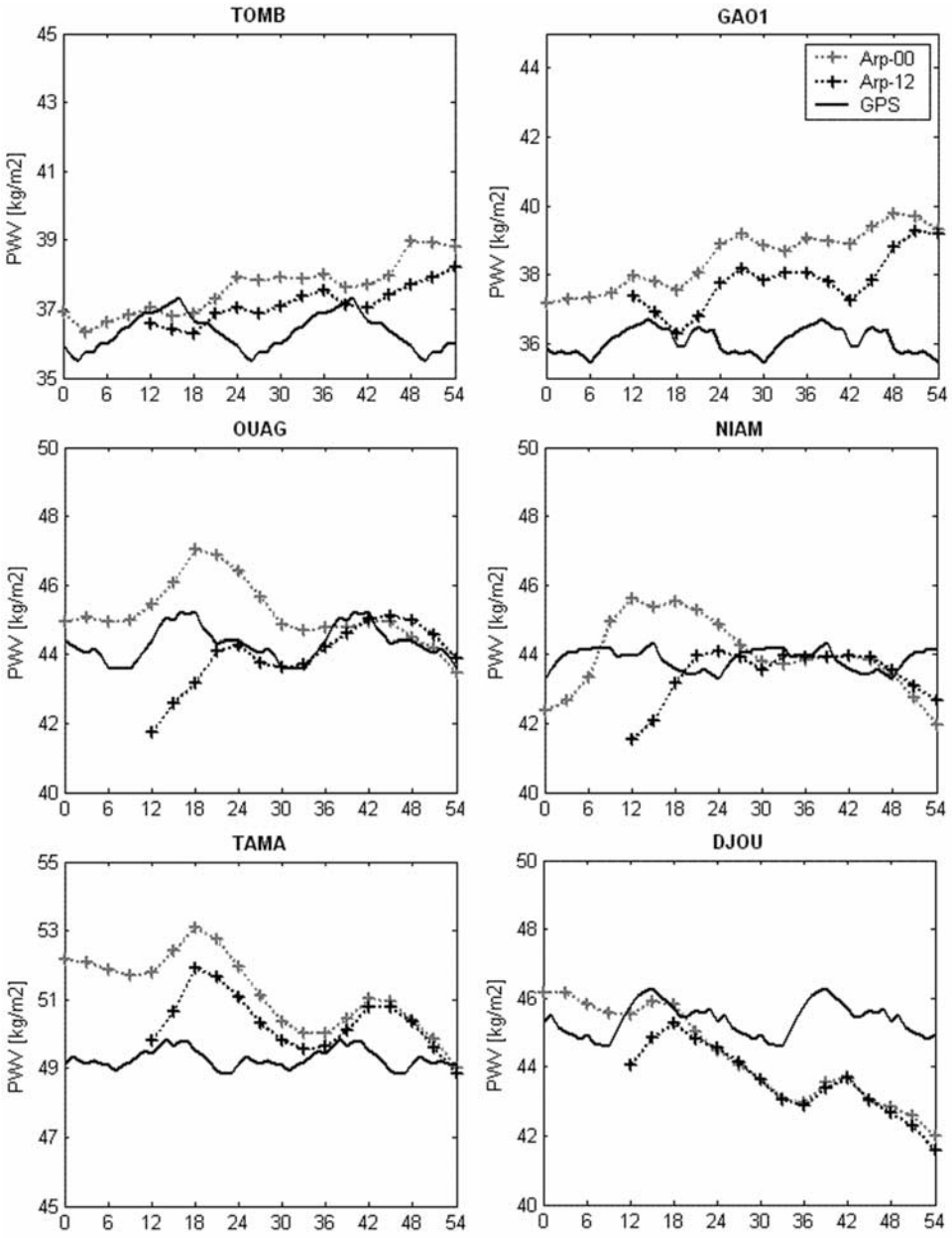

Figure 7. Mean values in PWV from ARPEGE operational model and precise/reprocessed GPS PWV estimates at the six AMMA GPS sites, computed over June-September 2006. The model data are plotted as dotted lines with plus signs, and GPS data are plotted as black solid lines. The gray (black) curves show the model forecasts initialized at 0000 (1200) UTC. The abscissa indicates the forecast time in hours since 0000 UTC. The GPS PWV estimates are reported hourly while model data are reported 3-hourly.

characterizing the diurnal cycle of the sonde errors and their dependence on sonde age.

5. Multiscale Analysis of PWV From GPS Data

5.1. Seasonal Cycle and Intraseasonal Variability

[21] A fundamental question is to understand which mechanisms precisely drive the seasonal migration of the WAM system and its intraseasonal variability (mainly active phases and pauses of rainfall). Figure 9 shows the seasonal evolution of precipitation and PWV for 2005 and 2006. The ITCZ can be seen as the region of high precipitation, with a maximum located over the ocean between January and April. In April-May, it is moving northward to 5°N, leading to the first rainy season over the Soudano-Guinean zone (5°N–10°N). According to *Sultan and Janicot* [2003], the ITCZ moves quickly to the north at the end of June. This monsoon jump (or onset), is preceded by a pause in rainfall over the whole region and followed by a restart of rainfall more to the North. It then leads to strong rainfall over the southern Sahel (10°N–15°N) while rainfall is reduced over

Table 4. Location of RS Stations, Type of Sondes, and Displacement With Regard to GPS sites[a]

RS Identification	Location	Type of Sonde 2005	Type of Sonde 2006	Latitude (°N)	Longitude (°E)	Altitude (m)	GPS Identification	Horizontal Displacement (km)	Vertical Displacement (m)
61052	Niamey[b]	RS80	RS92	13.5	2.2	227	NIAM	3	−4
61223	Tombouctou	None	RS80	16.7	357.0	263	TOMB	1	0
61641	Dakar[b]	RS80	RS80	14.7	342.5	24	DAKA	6	−8
65330	Parakou	None	MODEM	9.4	2.6	393	DJOU	110	43
65418	Tamale	None	RS92	9.6	359.2	168	TAMA	1	2
65503	Ouagadougou	RS80	MODEM	12.4	358.5	306	OUAG	1	−1

[a]Displacement: GPS – RS. Some sonde types changed between 2005 and 2006.
[b]In 2006, sonde types have been mixed (the types indicated for these sites are those used in this study).

the Guinean zone. This scheme applies well to the 2 years displayed in Figure 9. The onset date is defined by *Sultan and Janicot* [2003] as the center of the transition period (decrease in convection measured on the basis of OLR) between the end of the first rainy season on the Guinean coast and the beginning of the main rainy season over the Sahel. Hence, they find a mean climatological onset date of 24 June, while for the 2 years considered here they find: 22 June 2005 and 03 July 2006 (denoted as vertical bars in Figure 9). The onset date in 2005 is closer to the mean date than 2006. Compared to 2005, the evolution of rainfall in 2006 is characterized by less rainfall in the Soudano-Guinean zone in June and a long pause starting over Sahel on 15 June and ending around 10 July, i.e., 7 days after the onset date. The origin of these differences is not fully understood yet, but inspecting the evolution of atmospheric humidity may help identifying some of the mechanisms.

[22] A significant part of the moisture that precipitates over land is actually supplied by moisture convergence, while the remainder is produced by evapotranspiration from the surface [*Cadet and Nnoli*, 1987; *Fontaine et al.*, 2003]. The seasonal evolution of the rainbelt is thus tightly linked with that of atmospheric humidity. The seasonal evolution of PWV is shown in Figure 9 (left and right) on the basis of

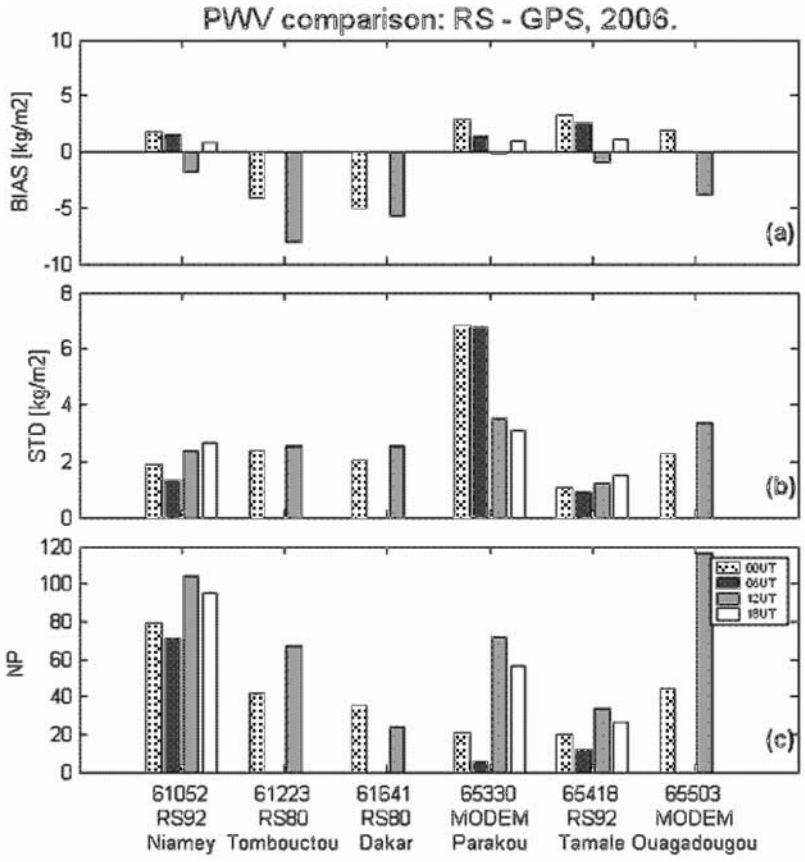

Figure 8. (a) Mean difference between RS PWV and GPS PWV, (b) standard deviation of difference, and (c) number of data pairs, at six collocated GPS-RS sites, for four times of day (0000, 0600, 1200, and 1800 UTC). High-resolution RS data have been used. The WMO codes of RS sites, sonde types, and locations of stations are indicated at bottom. The statistics are evaluated for the period June-September 2006, for nearly clear sky conditions only, to minimize the impact from rain and clouds (moist RS biases).

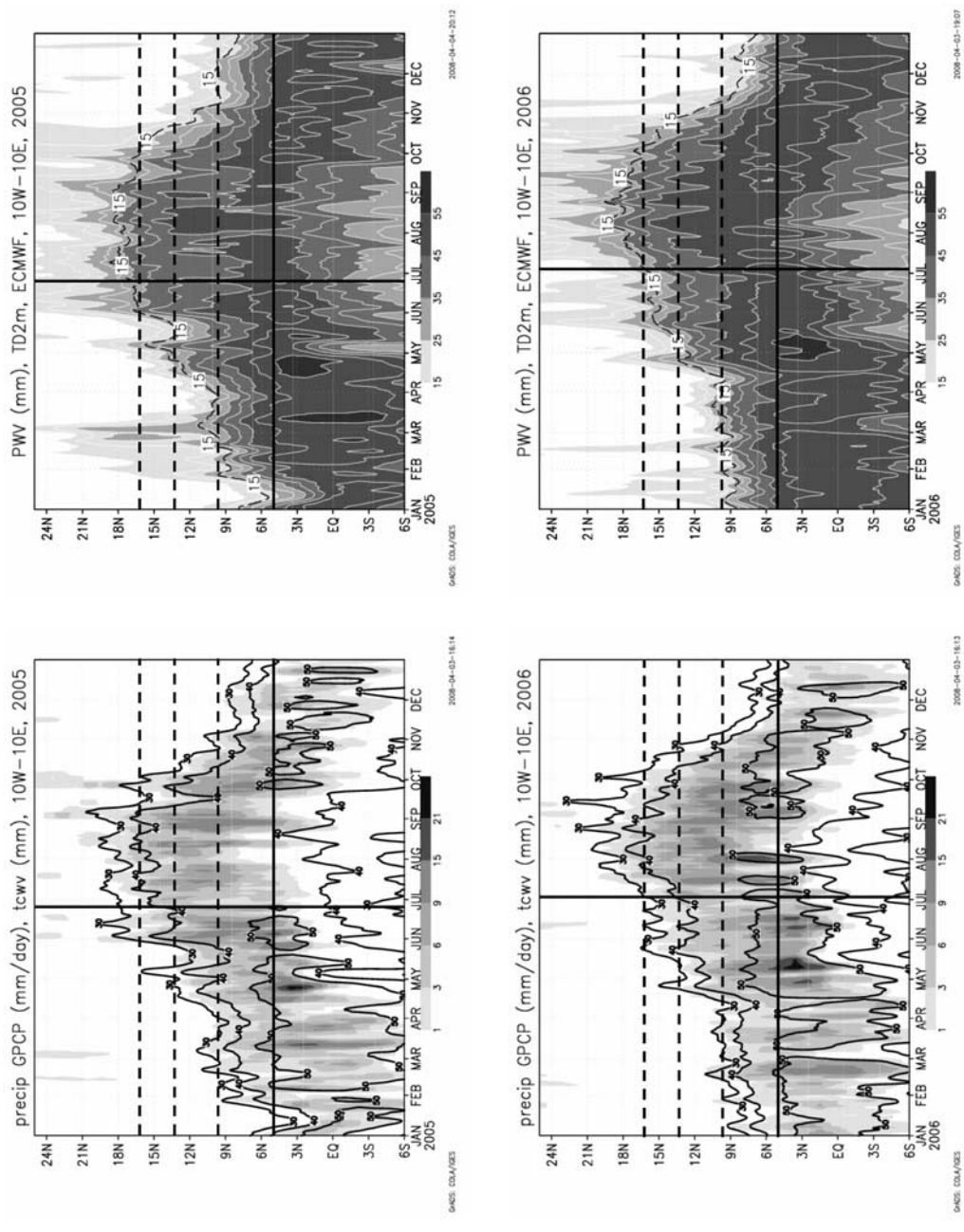

Figure 9. (left) Time-latitude diagrams of GPCP precipitation (shading) and (right) PWV from ECMWF operational analysis (shading) for (top) 2005 and (bottom) 2006. Superimposed are: (left) contours of PWV = 30, 40, and 50 kg m^{-2}, and (right) dew point temperature = 15°C at 2 m. All the data are zonally averaged over 10°W–10°E and smoothed with a 5-day running mean. The solid horizontal lines indicate the mean latitude of the coast (~5°N), the dashed horizontal lines indicate the latitudes of three AMMA GPS sites (Djougou, 9.7°N, Niamey, 13.5°N, and Gao, 16.3°N), and the solid vertical lines indicate the dates of onset (see text).

which we will first describe the overall evolution common to both years. Similar to precipitation, PWV shows a marked northward migration of the moist air mass leading to the monsoon season in the Sahel between July and September. Both variables are highly correlated, as revealed by the superimposition of PWV onto precipitation (Figure 9, left). The region where PWV > 50 kg m^{-2} delineates roughly the ITCZ, with local PWV maxima coinciding well with precipitation maxima. The region where PWV > 40 kg m^{-2}, has a broader meridional extension, roughly from equator to 15°N in August, which encompasses the whole rainbelt. The northern edge of the rainbelt is actually closely following the course of the atmospheric moisture, with a good correspondence between the 1 mm/day rainfall limit and the 30–40 kg m^{-2} PWV limit. Hence, there is a limit revealed in PWV (~35 kg m^{-2}) below which convection seems inhibited and no rainfall occurs. This might not exclusively be linked to total atmospheric moisture but also to the existence of adequate thermodynamical conditions (e.g., vertical distribution of humidity, convective availability, moisture convergence). Such a link, albeit apparently strong, has not been emphasized much so far. Indeed, several previous studies, focused on precipitating convection over West Africa, have rather highlighted a significance of midlevel dry air [e.g., *Roca et al.*, 2005]. One must note also that while the level of accuracy of existing satellite rainfall estimates and NWP analyses may presently allow for investigating the atmospheric water cycle at regional scale, this might not be the case for smaller but major scales (notably mesoscale and diurnal scales).

[23] Figure 9 (right) shows in more details the time and latitudinal evolution of PWV but also of the 15°C dew point temperature limit, which is often taken as the location of the intertropical discontinuity (ITD). It is highly correlated with the limit of PWV = 30–35 kg m^{-2}. Precipitation is mainly located to the South of this limit, in the moist monsoon flux, while to the North the dry northeasterly Harmattan winds and large-scale subsidence in the upper levels tend to inhibit moist convection. At intraseasonal timescales, correlated variability in precipitation, PWV and location of the ITD is also observed (Figure 9), especially with periodicities around 10–15 days (e.g., in June 2006) and 15–20 days (e.g., in August 2006). The inspection of point time series from GPS data will be very useful for investigating further this variability (see below).

[24] Though a number key ingredients of the mechanism leading to the northward migration of the WAM system are known, much is still unclear about their causality and interactions. The spectacular seasonal cycle (northward/southward migration) of the high PWV zone in Figure 9 is actually the result of several factors. In the lower levels (below 850 hPa), the main source of moisture is from the southwesterly moist monsoon flux, which advects horizontally moisture from Gulf of Guinea and tropical Atlantic Ocean [*Cadet and Nnoli*, 1987]. Moist air is also advected from the Atlantic Ocean from the northwest and the Mediterranean Sea from the northeast [*Semazzi and Sun*, 1997; *Fontaine et al.*, 2003]. However, evapotranspiration from the surface is another significant source (up to ~5 mm d^{-1} in August (A. Boone, personal communication, 2008)), which exhibits also a significant seasonal cycle, partly in response to the evolution of precipitation. In the upper levels (above 850 hPa), moisture is mainly transported westward in the African Easterly Jet (AEJ). The magnitude of the moisture flux in the 850- to 300-hPa layer can be significantly larger than in the low levels [*Cadet and Nnoli*, 1987]. The moisture in this layer has multiple sources: the Mediterranean Sea (a result of anticyclonic circulation over central and eastern North Africa), the Indian Ocean and Central Africa. The seasonal migration of the AEJ actually closely follows that of the PWV patterns seen in Figure 9, with the latitudinal location of the core of the AEJ coinciding roughly with the 40–45 kg m^{-2} limit in PWV (not shown). This suggests that the northern flank of the AEJ may play an important role in the net humidification of the upper levels over the Sahel. In fact, about 60–70% of PWV is located in the 850- to 300-hPa layer encompassing the AEJ. Strong vertical advection occurs in this layer, which is also partly induced by strong horizontal convergence in the low levels along the ITD. More insight into the vertical stratification of moisture fluxes nearby the ITD is given in section 5.2.

[25] The differences in the seasonal evolutions of precipitation and PWV between 2005 and 2006 (Figure 9) are thus probably linked with differences in atmospheric circulation and interaction with orography (P. Drobinski et al., On the late northward propagation of the West African monsoon in summer 2006 in the region of Niger/Mali, submitted to *Journal of Geophysical Research*, 2008) which induce differences in moisture convergence. As shown also by *Semazzi and Sun* [1997], interannual variability in atmospheric circulation might be larger than evapotranspiration from the surface in the water budget. If we focus on the PWV = 30 and 40 kg m^{-2} limits before the onset, we see that in 2005, a sharp increase in PWV occurs by the end of May which brings the PWV = 40 kg m^{-2} limit to 13.5°N and the PWV = 30 kg m^{-2} limit to 18°N. In 2006, these limits are farther south at the same time of year. After the onset, in 2005, the PWV = 40 kg m^{-2} limit is moving slightly northward while the PWV = 30 kg m^{-2} limit remains stationary. In 2006, both limits in PWV, and hence the precipitation zone, move significantly northward, up to 17°N and 20°N, respectively. This might explain the slightly higher amount of precipitation recorded in the Sahel in July-September in 2006. More insight into the intraseasonal variability can be gained from the inspection of time evolutions at the GPS sites.

[26] Figure 10 shows the seasonal evolution of PWV estimated at three GPS sites located along the meridional gradient of PWV and precipitation seen in Figure 9. PWV from operational ECMWF analyses and precipitation estimates from GPCP (Global Precipitation Climatology Project) are displayed as well. The differences between ECMWF PWV and GPS PWV are not the focus here, but one can notice the significant reduction in PWV bias in ECMWF analyses between 2005 and 2006. We believe this improvement is partly owing to substantial changes in the ECMWF operational model in February 2006, and to the unprecedented amount of additional observations that were assimilated into the model during the AMMA SOP (but notice that GPS data were not assimilated). Figure 10 shows that the PWV time series exhibit a large seasonal cycle at all sites which is correlated with the northward migration of the WAM system (Figure 9). The seasonal cycle in PWV as

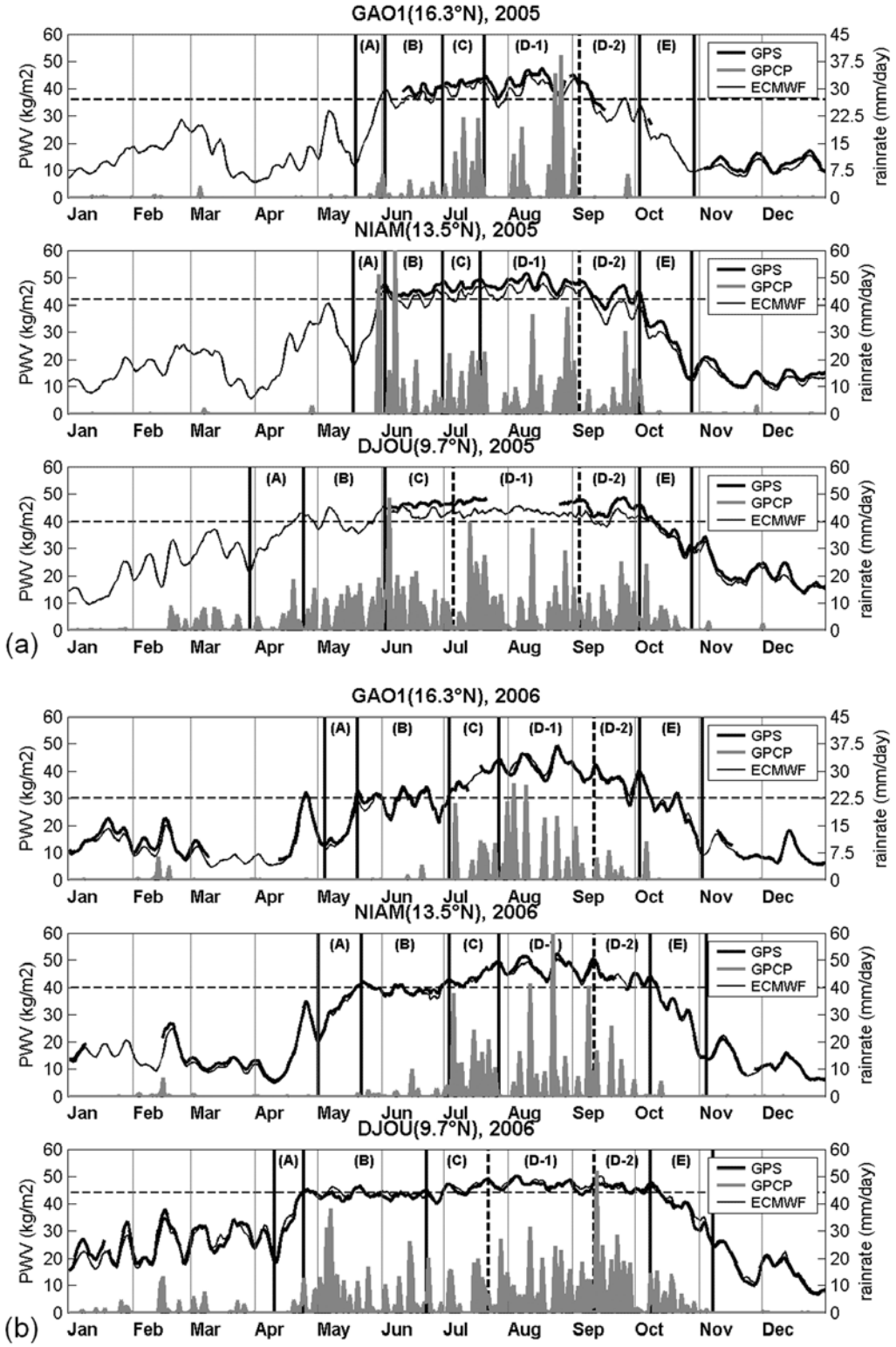

Figure 10. Time series of PWV (left-hand axis) and precipitation (right-hand axis) at stations (top) Gao, (middle) Niamey, and (bottom) Djougou, for (a) 2005 and (b) 2006. PWV estimates from GPS (thick black curves) and analyzed from ECMWF operational model (thin black curves) are smoothed with a 5-day running mean. ECMWF data are interpolated horizontally and corrected for the vertical displacement with respect to the GPS sites. Precipitation estimates (gray shaded areas) from GPCP 1-day-1-degree data set are extracted at the nearest grid point; they are not smoothed in time. The vertical lines delimit subperiods in the WAM seasonal cycle (see definition in the text); the horizontal dashed lines refer to the mean value during period B.

observed from these sites reveals clearly four periods: the dry period (November-March), the moist air mass installation period (April-June), the full monsoon (July-September) and the monsoon retreat (October). At Niamey and Gao, PWV values are typically below 10 kg m^{-2} during the dry period and above 40 kg m^{-2} during the wet period, while at Djougou the values are generally a bit larger (about 5 kg m^{-2}). The dry period, though being characterized by small PWV amounts, exhibits very large fluctuations associated with moisture advection over West Africa which origin can be from tropical Atlantic Ocean, Guinean Gulf and/or Mediterranean Sea. The PWV fluctuations during the wet season are comparatively much smaller, especially at Djougou, because the air then is close to and bounded by saturation.

[27] The monsoon season (April-October) is analyzed more precisely with an attempt to identify specific ''moisture-related'' subperiods. Therefore, and instead of using precipitation, we use here PWV for defining these subperiods. Namely, we distinguish periods of PWV increase and decrease, stationary phases and phases with marked variability. These PWV variations are indeed tightly linked with variations in moisture convergence, and hence with atmospheric circulation. Precipitation is overlaid to reveal the impact of these variations in terms of rainfall activity. Hence, we identified five subperiods, which are more or less well identified, depending on the site (i.e., on the latitude) and on the year considered. They are shown as vertical lines in Figure 10 (dotted vertical lines are used when the separation between subperiods is not evident). Period A corresponds to the installation of the humid air mass at each site. It is characterized by a significant increase in PWV, generally associated with the local passage of the ITD (see Figure 9, right). This takes place in April at Djougou and mid-May at Niamey and Gao. PWV reaches then a level of PWV $\geq$ 30 kg m^{-2} or 40 kg m^{-2} depending on the site and year. For both years, we can also notice large spikes in PWV before that period, which are also associated with displacements of the ITD. These can be observed in April-May at Niamey and Gao, and between February and March in Djougou. Again, the passage of the ITD at these sites corresponds to spikes in PWV exceeding PWV = 30 kg m^{-2}. Period A is followed by a stationary period B, where PWV remains around a threshold value, indicated by the dashed horizontal lines in Figure 10, during which some rainfall can occur. At Djougou, this period corresponds actually to the first rainy season over the Guinean coast (April-May). At Niamey, this period shows significant rainfall in 2005 but not in 2006, while at Gao, there is almost no rainfall. In 2006, the PWV at Gao exhibits strong oscillations with a 10- to 15-day period which is linked with close proximity of the ITD (see Figure 9) and is seen also in the meridian component of the wind at 925 and 850 hPa (not shown). Period C is characterized by a further increase in PWV around the monsoon onset, starting late June in 2005 and early July in 2006, at Niamey and Gao. This period is especially marked in 2006 with an increase in PWV of 15 kg m^{-2} at Gao and 10 kg m^{-2} at Niamey. At Djougou, such an increase in PWV does not occur. In fact, atmospheric relative humidity data provided by the relatively close RS site of Parakou suggest that water saturation is a major factor preventing significant PWV increase in Djougou (the lower atmospheric levels there are typically cooler than farther north). Significant rainfall accompanies this period at all sites, especially the northern ones where it corresponds to the beginning of the monsoon season. Period D covers the rest of the monsoon season during which PWV reaches its highest contents and the most heavy rainfall events are recorded at the northern sites (up to 40 mm at Niamey and 30 mm at Gao). We actually distinguish two subperiods (D-1 and D-2) which correspond to the core of the rainy season (August) and the start of the monsoon retreat (September), respectively. One of the significant characteristics of period D is the large variability in PWV and rainfall with a periodicity of 15–20 days for both years at Gao and Niamey. It is linked with similar variability in the meridian wind component between 925 and 700 hPa (not shown) and OLR [*Janicot et al.*, 2008]. This kind of signal can be assimilated to the intraseasonal variability (break and surge phases of rainfall) described by *Sultan et al.* [2003]. Finally, period E corresponds to the retreat of the monsoon during which the last rainfall events are observed.

[28] Inspection of both years separately shows that the start and end of the above periods are well phased between sites. The dates for Niamey and Gao almost perfectly coincide for all periods, and these coincide also to the dates for some of the periods (e.g., C, D, E) for Djougou. This fact indicates that the PWV contents observed at these sites are representative of large-scale atmospheric processes (mostly moisture advection). Moreover, the intraseasonal variability in PWV, especially during period D is shown to be highly correlated between all three sites. On the other hand, the phasing and duration of the periods exhibits significant interannual variability. Hence period A starts earlier in 2006 than in 2005 at the northern sites, while the start of period C, linked to the monsoon onset, is delayed in 2006. These results are consistent with the analysis of dynamical atmospheric fields for 2006 [*Janicot et al.*, 2008]. Another significant difference between both years is the level of PWV reached in period B, which was already seen in Figure 9. At Gao and Niamey, the mean PWV is about 30 and 40 kg m^{-2}, respectively, in 2006 and 36 and 42 kg m^{-2} in 2005, according to ECMWF analyses (the GPS estimates in fact yield even higher values in 2005). The origin of this smaller moisture content over the Sahel in 2006 is not presently explained, but might involve differences in atmospheric circulation. It is accompanied with smaller precipitation amounts in June 2006, especially at Niamey. At Djougou, the reverse is observed, with PWV being higher in 2006 than in 2005 (44 versus 40 kg m^{-2}) according to ECMWF analyses. However, there are no GPS data during period B in 2005 to validate this fact. It may actually not be so marked because of the bias seen in the analyses later (June-September 2005). Nevertheless, it is clear from Figure 9 that both the moist air mass and the rainbelt are located more to the south in June 2006 compared to June 2005. The reason of this feature requires further investigation as it might have played a significant role in the characteristics of the 2006 monsoon onset. The dates and magnitudes of PWV during the five subperiods, as well as PWV variations reached in each subperiod, appear thus as possible diagnostics for analyzing the interannual

variability of the characteristics of the WAM at intraseasonal timescales. Hence, we plan to repeat this analysis for other years in the near future.

[29] The marked seasonal variation in atmospheric humidity over West Africa (Figures 9 and 10) is the result of various processes acting either as sources (moisture convergence, surface evapotranspiration, and evaporation of precipitation) or sinks (moisture divergence, condensation and deposition), not mentioning vertical redistributions of moisture operated by boundary layer turbulence and convective transport. These processes act at different space scales and timescales and their efficiency varies seasonally and spatially. During the monsoon, and for timescales larger than 5–10 days, the lower troposphere is most largely controlled by the balance between large-scale advection and moist convective processes in the Soudano-Guinean zone while in the Sahelo-Saharan zone, the balance involves more significantly surface and turbulence processes at the expense of precipitating convective processes [*Peyrillé and Lafore*, 2007]. All these processes exhibit significant seasonal but also diurnal cycles. The next section discusses the latter.

5.2. Seasonal Evolution of the Diurnal Cycle

[30] The significance and role of the diurnal modulations of humidity in the atmosphere during the different phases of the monsoon are still rather unclear (e.g., the humidification before the onset, the interaction with moist convection during the core of the wet season). *Parker et al.* [2005] have shown that atmospheric circulation exhibits a significant diurnal cycle, with nocturnal southwesterly moisture advection in the planetary boundary layer (PBL) and vertical turbulent mixing during the daytime. This process is probably the most important in humidifying the atmosphere in the preonset period (A to C, in Figure 10). It is especially efficient in the regions of steep humidity gradient, i.e., close to the ITD. Whether this humidification exhibits a diurnal cycle in PWV is not evident because the total column water vapor is conserved in the absence of moisture sinks.

[31] The high-resolution GPS PWV data provide a unique opportunity to investigate the diurnal cycle in PWV. Actually, very few studies have focused so far on the diurnal cycle of the lower tropospheric humidity, mainly owing to lack of observational data and significant uncertainties in numerical model simulations at this timescale (section 4). *Bock et al.* [2007a] have shown that the diurnal cycle in PWV is rather small at Dakar compared to equatorial and midlatitude sites. However, in section 4 we have shown that a diurnal signal in PWV can be observed on average over the monsoon season at the six GPS sites covering the Soudanian and Sahelian regions (see Figure 7). We discuss below the seasonal evolution of the diurnal cycle in PWV at these sites and its link with atmospheric processes described by *Parker et al.* [2005] and *Peyrillé and Lafore* [2007].

[32] Figure 11 shows monthly composites of diurnal cycle of specific humidity at 2 m (q_{2m}) and PWV at the three EOP GPS sites considered in section 5.1. A coherent diurnal signal in both variables is observed at all three sites, as already seen for the wet-season average of PWV in Figure 7. Both variables exhibit a significant diurnal modulation during two preferential periods of the year, which differ slightly as a function of the latitude of the site. At Djougou, the q_{2m} anomalies are largest in March-April and November, respectively. At Niamey and Gao, they peak in May-June and September-October. The PWV anomalies are actually more or less coincident with q_{2m} anomalies at Niamey and Gao, but not at Djougou. At all sites, the q_{2m} anomalies occur thus during periods A and E when the ITD is close to the site (i.e., during the period of local monsoon onset and retreat; see Figure 9). The peaking periods tend to merge together when moving from the southern to the northern site (i.e., when the rainy season becomes shorter).

[33] Apart from these similarities, there is a significant difference between q_{2m} anomalies and PWV anomalies. The PWV anomalies exhibit a marked seasonal evolution in the times of maximum and minimum, while the q_{2m} anomalies have fixed times of maximum (0600–0800 UTC) and minimum (1400–1600 UTC). At Djougou the PWV minimum occurs between 0300 and 0800 UTC between March and November and the time of maximum is shifting from 0100 UTC in April to 1500 UTC in August and then back to 2000 UTC in November. At Niamey, these timings are significantly different. The minimum of PWV is located at 2000–2200 UTC in May-June and 0000–0200 UTC in September, and the maximum is shifting extending between 1400 UTC in April to 0500 UTC in June and back to 1200–1400 UTC between August and November. At Gao, the patterns of PWV maximum and minimum are rather unorganized, but nevertheless indicate that the PWV maximum occurs in the afternoon, while the minimum occurs during night.

[34] At all sites, there is thus a contrast between the well organized q_{2m} anomalies and the less well organized PWV anomalies. This reflects that the moisture sources and sinks in the atmospheric column are not simply related to near surface processes. In fact, the maxima in q_{2m} anomalies at 0800 UTC and minima at 1600 UTC are fairly consistent with the mechanism of nocturnal moisture advection and daytime boundary layer convective mixing above a dry surface. Thus the vertical mixing is especially effective in drying the low levels (and q_{2m}) when surface evapotranspiration is low and the free troposphere dryer such as during monsoon onset and retreat. During the core of the rainy season, the air is closer to saturation. For example, at Djougou, the relative humidity at 2 m remains above 90% between 0000 and 0600 UTC in August (not shown). In contrast, the PWV is not only related to near surface or boundary layer moist processes but also to the humidity in the free troposphere.

[35] Inspection of monthly mean radiosonde profiles and UHF wind profilers reveals that three layers are participating to the diurnal modulation of moisture advection [*Lothon et al.*, 2008]. We can namely identify: a nocturnal low-level jet (NLLJ), developing throughout the night and extending from the surface up to ~1200 m above the ground level (agl) at Niamey, the AEJ layer, between 2 and 5 km agl, and an intermediate layer between 1200 and 2000 m agl (already highlighted by *Parker et al.* [2005]) characterized by a northerly wind component. Figure 12 shows profiles of moisture fluxes and humidity, for the month of May in Niamey, i.e., prior to the monsoon onset, when the surface is dry and the ITD relatively close to this site (Figure 9). These layers can be clearly distinguished. Because of the significant humidity biases evidenced in radiosonde data in

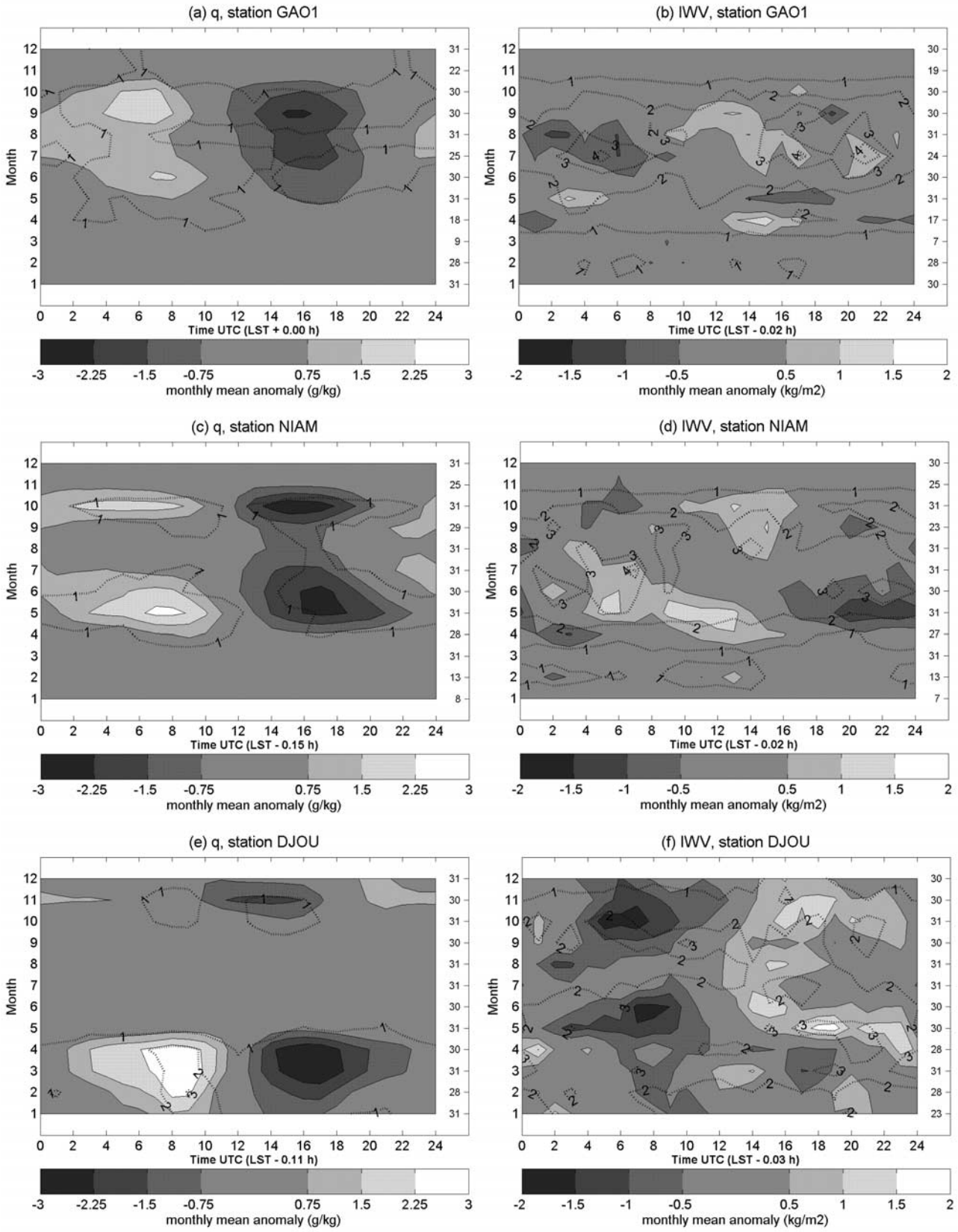

Figure 11. Diurnal cycle of monthly mean anomalies of (left) specific humidity at 2 m and (right) GPS PWV. The horizontal axis in each plot indicates time UTC (time shift with regard to mean local solar time is indicated) and the vertical axis indicates month of year 2006. The number of days used is indicated on the right vertical axis.

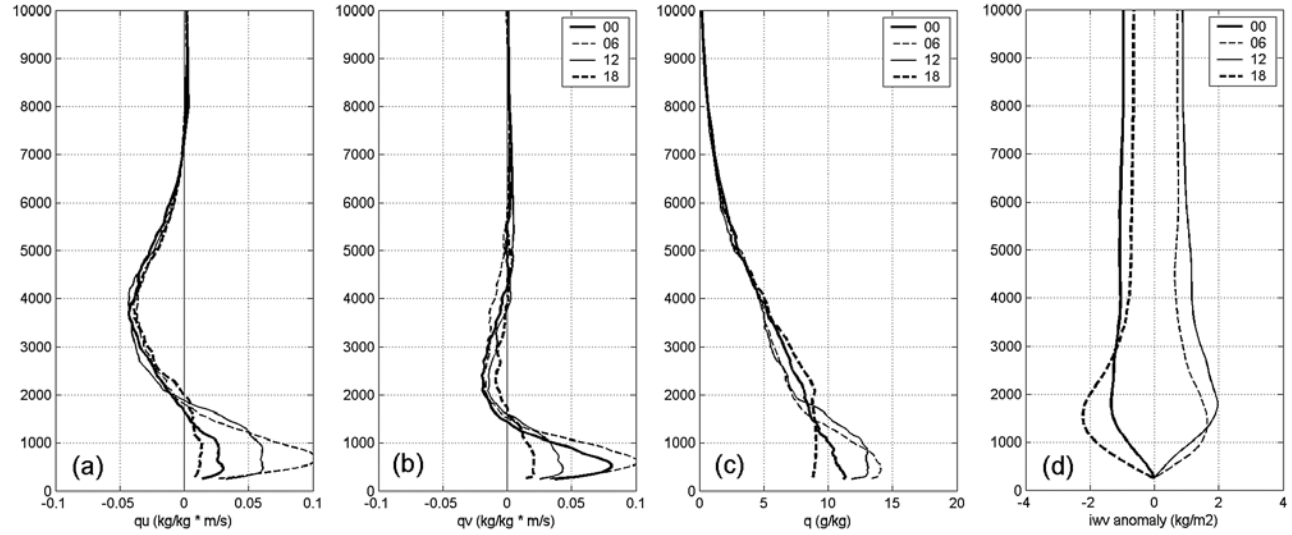

Figure 12. Radiosonde profiles averaged over the month of May 2006 at Niamey: (a) zonal and (b) meridional moisture flux, (c) specific humidity, and (d) PWV integrated from the surface to level z. The humidity profiles have been adjusted to fit the total PWV values measured by GPS.

section 4, we used only RS92 data and adjusted the humidity profiles to fit the PWV values derived from the GPS data. Therefore, we performed a simple 1D-Var assimilation of GPS PWV with the radiosonde specific humidity profile serving as first guess. The vertical correction is controlled by the distributions of errors in the first-guess (we assumed that $\sigma_q(z) = q(z)$) and GPS observation (σ_{PWV} being converted from the formal ZTD errors discussed in section 3, $\sigma_{PWV} = \kappa(T_m) \times \sigma_{ZTD}$). This correction can change significantly the humidity profiles in the PBL (but this is not so strong for the month of May shown here). The comparison of humidity at the lowest level to q_{2m} (here an independent observation) gives good confidence in the corrected profiles. Though this correction may not be perfect, it has the advantage of being consistent with the GPS PWV anomalies shown in Figure 11 and help identifying the impact of stability, vertical stratification and advection.

[36] The profiles in Figure 12 show that humidity is peaking in the PBL at 0600 UTC, as a result of strong moisture advection from the NLLJ (indeed, the maximum is peaking well above the ground level, and this monthly mean feature is actually found in many individual profiles). The moisture flux is mainly southerly at 0000 and southwesterly at 0600 UTC, as the NLLJ turns clockwise from south to southwest. It is located in a thin layer at ~400 m agl. The signature at the surface of the NLLJ is explained by shear-driven downward turbulent mixing (Lothon et al., submitted manuscript, 2008). Some mixing is likely to occur upward and to contribute to the humidification of the Saharan layer. Indeed, from the NLLJ maximum to about 1200 m the shear is still significant and the thermal stratification somewhat weaker, while above in the Saharan layer, the shear weakens but this layer remains consistently much closer to neutral. During daytime, the development of the convective PBL flushes the moisture in this layer through vertical mixing [*Parker et al.*, 2005]. Between 0600 and 1800 UTC, the specific humidity actually decreases uniformly from 13 to 8 g kg^{-1} in the lower part of the daytime PBL (0–2 km), while it increases above in the Saharan layer, up to an altitude of 4 km (albeit not homogeneously, this partly results from a variety of heights reached by well mixed layers at 1800 UTC in May, ranging typically from 2 to 4 km). Nevertheless, PWV is not conserved as it is seen to decrease from a maximum at 0600–1200 UTC to a minimum at 1800–0000 UTC (Figure 11). The PWV profile in Figure 12 shows that in the PBL, PWV is the largest at 0600 and the smallest at 1800 UTC, while when integrated over the total column, these peaks change to 1200 and 0000 UTC, respectively. The inversion occurs in the intermediate layer where the PWV anomalies are actually the largest (reaching more than ± 2 kg m^{-2}). The origin of this decrease in PWV is most likely due to a combination of dry air advected from the North (the Harmattan accelerates during night [*Peyrillé and Lafore*, 2007]) and the westward transport in the AEJ. The diurnal cycle of these two jets may thus play a significant role, in addition to the NLLJ, in controlling the humidification of the troposphere before the monsoon onset. Inspection of the other months at Niamey (not shown) reveals that the moisture flux in these jets is very weak in April (consistent with a very small diurnal cycle in PWV), while it is strengthening in the AEJ between June and September. The southward moisture flux in the return flow is slightly smaller in June-July and September than in May, and vanishes in August (consistent with respective diurnal cycles in PWV).

[37] A similar inspection of vertical profiles has been performed from radiosonde data at Parakou and Tamale adjusted to fit the GPS PWV data from Djougou and Tamale, respectively (not shown). The diurnal phasing there is however significantly different from the one at Niamey, though the influence of the AEJ and the return flow could be established. At these more southerly sites, the interaction with surface fluxes, increased evapotranspiration, convection and precipitation probably play an important role on the phasing of the PWV anomalies. The northernmost sites of Gao and Tombouctou could not be analyzed in a similar way because there are either no radiosoundings (Gao) or to

few in 2006 (Tombouctou). A more extended investigation at some of these sites will be presented in a future publication.

[38] There are several important questions still open, however, regarding the importance of evapotranspiration from the surface and evaporation of precipitation on the lower tropospheric water budget and the interaction between tropospheric moisture and convection. The afternoon PWV peak is in fact broadly consistent with the diurnal phasing and expected magnitudes of evapotranspiration. On the other hand, convection over West Africa is known to exhibit a strong diurnal cycle [*Toledo Machado et al.*, 1993]. During the monsoon season, deep convection develops in the afternoon while precipitation is maximum during the nighttime hours [*Yang and Slingo*, 2001; *Mohr*, 2004]. This phasing seems correlated with PWV diurnal variations, as well, namely the convection peak is coincident with a peak in PWV and precipitation is followed by a decrease in PWV. Inspection of high temporal resolution GPS PWV and precipitation data reveals that moderate and strong rain events are nearly systematically accompanied by large spikes in PWV of ~ 5 kg m^{-2} which last a few hours only (e.g., Figure 6). Understanding the details of this mechanism needs further investigation, using both observations and numerical simulations of convective events.

6. Conclusions and Perspectives

[39] This paper introduced the GPS network deployed in the framework of AMMA thanks to the involvement of many institutions and people cosigning this paper. Different GPS data processing schemes have been developed for various applications such as near-real time NWP model forecast verification and climate studies using a reprocessed data set. Using state-of-the-art GPS data processing, the accuracy for a single PWV estimate is assumed to be smaller than 1.5 kg m^{-2}, with a possible bias that is believed to be at the level of $\pm$ 0.5 kg m^{-2}. The bias might be station-dependent and linked with multipath, antenna phase center variations, and residual tropospheric model errors. Near real-time and rapid (processed next day) GPS solutions have been evaluated using the precise reprocessed data set. They showed some scatter and outliers (1.1–2.3 kg m^{-2} at one standard deviation), but still proved useful for NWP model verifications in near real time.

[40] Significant deficiencies in NWP model forecasts are evidenced using the precise/reprocessed data set (such as a diurnal trend in PWV seen in Figure 7). They are believed to be linked to physical parameterizations and, in some cases, are enhanced by specific features of the assimilation scheme. Biases in the 0000 and 1200 UTC analyses, and offsets between the analyses and forecasts at 1200 UTC, are found at four sites at which radiosonde data were assimilated. At these sites, consistent systematic biases are also found in the radiosonde data (Figure 8), which obviously influenced the quality of the NWP analyses, consistently with previous studies [*Bock et al.*, 2007b]. Among the three types of radiosondes evaluated with the help of GPS PWV estimates, Vaisala RS80 sites showed the largest dry biases (up to 8 kg m^{-2} or 25% of PWV). The MODEM and Vaisala RS92 sites showed smaller biases, but with a marked day/night variation (3–4 kg m^{-2}) in the bias. Compared to GPS PWV, these radiosondes show a wet bias during night and a dry bias during day (most likely due to solar radiation). These results are consistent with those of *Wang and Zhang* [2008].

[41] The GPS PWV estimates will be further used for verifying the radiosonde correction schemes developed at CNRM [*Nuret et al.*, 2008] and ECMWF as well as the AMMA reanalysis [*Agusti-Panareda and Beljaars*, 2008]. Both the corrected radiosonde data and NWP models are of prime importance for water budget studies. Another perspective to be considered beyond AMMA is the use of an operational GPS network over West Africa for verifying in near real-time the radiosonde and NWP models as illustrated in Figure 6. If such a network could be operated, the assimilation of GPS ZTD or PWV data into the NWP models would probably be beneficial for improving medium range weather forecasts.

[42] In section 5, we have shown that the seasonal evolution of PWV is tightly linked with that of the rainbelt over West Africa, as already pointed out by *Takiguchi et al.* [2000], over the Pacific area, and *Kursinski et al.*, 2008, over North America. Different critical levels in PWV appeared, revealing namely that almost no precipitation occurs when PWV is below 30 kg m^{-2}. This limit is actually closely related with the location of the ITD and shows marked intraseasonal variability. Another limit, PWV = 40 kg m^{-2}, seems related to the monsoon onset, as defined on the basis of OLR by *Sultan and Janicot* [2003]. More generally, the spatiotemporal variability in PWV seems a good tracer of atmospheric circulation, revealing both activity in the low levels (mainly the monsoon flux) and upper levels (mainly the AEJ). This can be easily understood since West Africa is characterized by a strong meridian gradient in humidity (Figure 9), hence any perturbation in the atmospheric flow is likely to advect dry or moist air.

[43] The GPS PWV estimates have been used in an Eulerian analysis of PWV variability at intraseasonal timescales. Five periods could be distinguished in the overall monsoon season (April to October) at all GPS sites. According to this stratification, we characterize the season by: (period A) the installation of the moist air mass (linked with the northward migration of the ITD), (period B) a stationary period during which shallow convection tends to moisten the upper levels (consistent with the 2D simulations, Peyrillé and Lafore, personal communication), (period C) the monsoon onset period during which the moist air mass is shifting more to the North and rainfall starts in the Sahel, (period D) a period of marked intraseasonal variability with 10–20 day oscillations in PWV content and precipitation such as described by *Sultan et al.* [2003], (period E) the monsoon retreat. The comparison of years 2005 and 2006 shows that this diagnostic seems robust and might be used for analyzing interannual variability. The most significant differences between these 2 years are observed during periods A to C, consistently with the delayed onset in 2006 diagnosed by *Janicot et al.* [2008]. Hence year 2006 compared to 2005 is characterized by: significantly smaller PWV shifts in Niamey and Gao during period A, thus reaching smaller PWV contents with almost no precipitation during period B, period B is longer at all sites, and

cumulated precipitation is significantly smaller at Djougou during period C.

[44] At shorter timescales, we also showed that there is a strong correlation between PWV variations and precipitation down to the scale of individual convective events (Figure 6). One timescale not discussed in this paper is that of the 3–10 days, including namely African Easterly Waves [*Redelsperger et al.*, 2002] and planetary waves [*Sultan et al.*, 2003]. The signature of such propagative disturbances in atmospheric humidity has been shown previously [*Cadet and Nnoli*, 1987; *Bock et al.*, 2007a]. They will be addressed in a future publication for the AMMA years.

[45] Diurnal cycle composites of GPS PWV, 2-m humidity and vertical profiles of horizontal wind components and humidity from radiosondes revealed a significant diurnal oscillation in these parameters with a marked seasonal evolution. However, the diurnal oscillation in PWV is comparatively smaller. It reaches ± 1.5 kg m^{-2} during periods A and B when the ITD is the closest. This signature results from the balance of water vapor transport in three layers, the nocturnal low-level jet, the AEJ, and the northerly return flow in between, as well as vertical mixing in the convective PBL. The mechanism of moisture advection by the NLLJ and vertical mixing during daytime described by *Parker et al.* [2005] is verified from these data, and seems especially active close to the ITD before the onset. During the core of the rainy season, surface latent heat fluxes, deep convection and precipitation are expected to complicate the interactions. This may explain the less organized and reduced magnitude of the diurnal anomalies in PWV.

[46] This work poses a preliminary diagnostic on the evolution of water vapor and precipitation over West Africa with emphasis on a broad range of timescales, from seasonal to diurnal. It is now necessary to investigate in more details the mechanisms that operate at all these timescales. The seasonal evolution and intraseasonal variability are tightly linked with atmospheric circulation. Hence it is necessary to investigate how moisture fluxes and convergence evolve, and which processes control them, knowing that at least three layers are actively participating to the transport of water vapor. The role of evapotranspiration from the surface may also be important at this stage. Another questioning concerns the role and efficiency of the diurnal cycle in humidifying the atmosphere before the onset, and the interaction between MCSs and humidity in their close environment during the core of the wet season. Finally, once the mechanisms are identified, they may also shed some light on the origin of interannual variability.

[47] **Acknowledgments.** On the basis of French initiative, AMMA was built by an international scientific group and is currently funded by a large number of agencies, especially from France, UK, U.S. and Africa. It has been the beneficiary of a major financial contribution from the European Community's Sixth Framework Research Programme. Detailed information on scientific coordination and funding is available on the AMMA International website http://www.amma-international.org. The GPS systems have been funded by INSU/CNRS, France, under program API-AMMA. The authors would like to acknowledge the following institutions and people for providing scientific, technical and administrative support in the installation and maintenance of the AMMA GPS network: National Meteorological Services (DMNs), ASECNA, ACMAD: (Mali) B. Diarra, M. Diarra., M. Konaté, S. Sekou, A. Touré, B.O. Traoré, Y. Traoré, and T.O. Traoré; (Niger) A. Abani, I. Daba Sabi, M.-C. Dufresne, A. Hassane, and E. Kenne; (Burkina-Faso) D. Alassane, L. Bougma, A.J. Garane, Y. Pafadnam, B. Theoro, and H. Yacouba; Ghana Met. Agency (GMA): D. Iddrissu, Z. Minia, and G. Wilson; Université Abomey-Calavi: Erik and Etienne Houngninou; IRD: F. Cazenave L. Descroix, A. Diedhiou, J. Dossougoin, S. Galle, J.P. Guengant, C. Kane, T. Lebel, A. Mariscal, D. Ouattara, C. Peugeot, Y.M. Prével, J.L. Rajot, J. Seghieri, J. Sogba-Goh, H. Tahirou Bana, and F. Timouk; IGN: J. Beilin, T. Duquesnoy, E. Fourestier, A. Harmel, C. Meynard, P. Nicolon, and J.-C. Poyard; Meteo-France: N. Asencio, F. Favot, L. Fleury, S. Legouis, and E. Brauge; CNRS: C. Flamant, E. Mougin, K. Ramage, J.-L. Redelsperger, M. Schaldembrand, and P. Weill.

References

Agusti-Panareda, A., and A. Beljaars (2008), ECMWF's contribution to AMMA, *ECMWF Newsl.*, *115*, 19–27.

Altamimi, Z., X. Collilieux, J. Legrand, B. Garayt, and C. Boucher (2007), ITRF2005: A new release of the International Terrestrial Reference Frame based on time series of station positions and Earth Orientation Parameters, *J. Geophys. Res.*, *112*, B09401, doi:10.1029/2007JB004949.

Baltink, H. K., H. van der Marel, and A. G. A. van der Hoeven (2002), Integrated atmospheric water vapour estimates from a regional GPS network, *J. Geophys. Res.*, *107*(D3), 4025, doi:10.1029/2000JD000094.

Betts, A. K., and C. Jakob (2002), Evaluation of the diurnal cycle of precipitation, surface thermodynamics, and surface fluxes in the ECMWF model using LBA data, *J. Geophys. Res.*, *107*(D20), 8045, doi:10.1029/2001JD000427.

Bevis, M., S. Businger, S. Chiswell, T. A. Herring, R. A. Anthes, C. Rocken, and R. H. Ware (1994), GPS meteorology: Mapping zenith wet delay onto precipitable water, *J. Appl. Meteorol.*, *33*, 379–386, doi:10.1175/1520-0450(1994)033<0379:GMMZWD>2.0.CO;2.

Bock, O., F. Guichard, S. Janicot, J. P. Lafore, M.-N. Bouin, and B. Sultan (2007a), Multiscale analysis of precipitable water vapor over Africa from GPS data and ECMWF analyses, *Geophys. Res. Lett.*, *34*, L09705, doi:10.1029/2006GL028039.

Bock, O., M.-N. Bouin, A. Walpersdorf, J. P. Lafore, S. Janicot, F. Guichard, and A. Agusti-Panareda (2007b), Comparison of ground-based GPS precipitable water vapour to independent observations and Numerical Weather Prediction model reanalyses over Africa, *Q. J. R. Meteorol. Soc.*, *133*, 2011–2027, doi:10.1002/qj.185.

Boehm, J., B. Werl, and H. Schuh (2006a), Troposphere mapping functions for GPS and very long baseline interferometry from ECMWF operational analysis data, *J. Geophys. Res.*, *111*, B02406, doi:10.1029/2005JB003629.

Boehm, J., A. Niell, P. Tregoning, and H. Schuh (2006b), Global Mapping Function (GMF): A new empirical mapping function based on numerical weather model data, *Geophys. Res. Lett.*, *33*, L07304, doi:10.1029/2005GL025546.

Boehm, J., R. Heinkelmann, and H. Schuh (2007), Short note: A global model of pressure and temperature for geodetic applications, *J. Geod.*, *81*(10), 679–683, doi:10.1007/s00190-007-0135-3.

Cadet, D. L., and N. O. Nnoli (1987), Water vapour transport over Africa and the Atlantic Ocean during summer 1979, *Q. J. R. Meteorol. Soc.*, *113*, 581–602, doi:10.1256/smsqj.47608.

Dai, A., and J. Wang (1999), Diurnal and semi-diurnal tides in global surface pressure, *J. Atmos. Sci.*, *56*, 3874–3891, doi:10.1175/1520-0469(1999)056<3874:DASTIG>2.0.CO;2.

d'Orgeval, T., J. Polcher, and L. Li (2005), Uncertainties in modelling future hydrological change over West Africa, *Clim. Dyn.*, *26*, 93–108, doi:10.1007/s00382-005-0079-3.

Drusch, M., and P. Viterbo (2007), Assimilation of screen-level variables in ECMWF's integrated forecast system: A study on the impact on the forecast quality and analyzed soil, *Mon. Weather Rev.*, *135*, 300–314, doi:10.1175/MWR3309.1.

Fontaine, B., P. Roucou, and S. Trzaska (2003), Atmospheric water cycle and moisture fluxes in the West African monsoon: Mean annual cycles and relationship using NCEP/NCAR reanalysis, *Geophys. Res. Lett.*, *30*(3), 1117, doi:10.1029/2002GL015834.

Ge, M., E. Calais, and J. Haase (2002), Sensitivity of zenith total delay accuracy to GPS orbit errors and implications for near-real-time GPS meteorology, *J. Geophys. Res.*, *107*(D16), 4315, doi:10.1029/2001JD001095.

Haase, J. S., M. Ge, H. Vedel, and E. Calais (2003), Accuracy and variability of GPS tropospheric delay measurements of water vapor in the western Mediterranean, *J. Appl. Meteorol.*, *42*, 1547–1568.

Hagemann, S., L. Bengtsson, and G. Gendt (2003), On the determination of atmospheric water vapor from GPS measurements, *J. Geophys. Res.*, *108*(D21), 4678, doi:10.1029/2002JD003235.

Janicot, S., et al. (2008), Large-scale overview of the summer monsoon over West and central Africa during the AMMA field experiment in 2006, *Ann. Geophys.*, *26*, 2569–2595.

King, R. W., and Y. Bock (2005), Documentation for GAMIT GPS analysis software, release 10.2, report, Mass. Inst. of Technol., Cambridge.

Kursinski, E. R., R. A. Bennett, D. Gochis, S. I. Gutman, K. L. Holub, R. Mastaler, C. Minjarez Sosa, I. Minjarez Sosa, and T. van Hove (2008), Water vapor and surface observations in northwestern Mexico during the 2004 NAME Enhanced Observing Period, *Geophys. Res. Lett.*, *35*, L03815, doi:10.1029/2007GL031404.

Le Barbé, L., T. Lebel, and D. Tapsoba (2002), Rainfall variability in West Africa during the years 1950–90, *J. Clim.*, *15*, 187–202, doi:10.1175/1520-0442(2002)015<0187:RVIWAD>2.0.CO;2.

Lebel, T., A. Diedhiou, and H. Laurent (2003), Seasonal cycle and interannual variability of the Sahelian rainfall at hydrological scales, *J. Geophys. Res.*, *108*(D8), 8389, doi:10.1029/2001JD001580.

Li, H., and B. Chen (2005), The evolution of precipitable water associated with the Asian and Australian monsoons as revealed from MODIS/SSM/I, ECMWF and NCEP reanalysis data sets, *Geophys. Res. Lett.*, *32*, L10811, doi:10.1029/2005GL022570.

Lothon, M., F. Saïd, F. Lohou, and B. Campistron (2008), Observation of the diurnal cycle in the low troposphere of West Africa, *Mon. Weather. Rev.*, *136*, 3477–3500, doi:10.1175/2008MWR2427.1.

Louvet, S., B. Fontaine, and P. Roucou (2003), Active phases and pauses during the installation of the West African monsoon through 5-day CMAP rainfall data (1979–2001), *Geophys. Res. Lett.*, *30*(24), 2271, doi:10.1029/2003GL018058.

Lyard, F., F. Lefevre, T. Letellier, and O. Francis (2006), Modelling the global ocean tides: A modern insight from FES2004, *Ocean Dyn.*, *56*, 394–415, doi:10.1007/s10236-006-0086-x.

Matthews, A. (2004), Intraseasonal variability over tropical Africa during northern summer, *J. Clim.*, *17*, 2427–2440, doi:10.1175/1520-0442(2004)017<2427:IVOTAD>2.0.CO;2.

Mohr, K. (2004), Interannual, monthly, and regional variability in the wet season diurnal cycle of precipitation in sub-Saharan Africa, *J. Clim.*, *17*, 2441–2453, doi:10.1175/1520-0442(2004)017<2441:IMARVI>2.0.CO;2.

Mounier, F., G. N. Kiladis, and S. Janicot (2007), Analysis of the dominant mode of convectively coupled Kelvin waves in the West African Monsoon, *J. Clim.*, *20*, 1487–1503, doi:10.1175/JCLI4059.1.

Niell, A. E. (1996), Global mapping functions for the atmosphere delay at radio wavelengths, *J. Geophys. Res.*, *101*, 3227–3246, doi:10.1029/95JB03048.

Niell, A. E., A. J. Coster, F. S. Solheim, V. B. Mendes, P. C. Toor, R. B. Langley, and C. A. Upham (2001), Comparison of measurements of atmospheric wet delay by radiosonde, water vapor radiometer, GPS, and VLBI, *J. Atmos. Oceanic Technol.*, *18*, 830–850, doi:10.1175/1520-0426(2001)018<0830:COMOAW>2.0.CO;2.

Nuret, M., J.-P. Lafore, O. Bock, F. Guichard, A. Agusti-Panareda, J.-B. Ngamini, and J.-L. Redelsperger (2008), Correction of humidity bias for Vaïsala RS80 sondes during AMMA 2006 Observing Period, *J. Atmos. Oceanic Technol*, doi:10.1175/2008JTECHA1103.1, in press.

Pacione, R., and F. Vespe (2003), GPS zenith total delay estimation in the Mediterranean area of climatological and meteorological applications, *J. Atmos. Oceanic Technol.*, *20*, 1034–1042, doi:10.1175/1520-0426(2003)20<1034:GZTDEI>2.0.CO;2.

Parker, D. J., R. R. Burton, A. Diongue-Niang, R. J. Ellis, M. Felton, C. M. Taylor, C. D. Thorncroft, P. Bessemoulin, and A. M. Tompkins (2005), The diurnal cycle of the West African monsoon circulation, *Q. J. R. Meteorol. Soc.*, *131*, 2839–2860, doi:10.1256/qj.04.52.

Petrov, L., and J.-P. Boy (2004), Study of the atmospheric pressure loading signal in very long baseline interferometry observations, *J. Geophys. Res.*, *109*, B03405, doi:10.1029/2003JB002500.

Peyrillé, P., and J.-P. Lafore (2007), An idealized two-dimensional framework to study the West African Monsoon. Part II: Large-scale advection and the diurnal cycle, *J. Atmos. Sci.*, *64*, 2783–2803, doi:10.1175/JAS4052.1.

Ramel, R., H. Gallee, and C. Messager (2006), On the northward shift of the West African monsoon, *Clim. Dyn.*, *26*, 429–440, doi:10.1007/s00382-0050093-5.

Ray, J., Z. Altamimi, T. Van Dam, and T. Herring (2007) Principles for conventional contributions to modeled station displacements, paper presented at IERS Workshop on Conventions, Bur. Int. des Poids et Mesures, Sèvres, France.

Redelsperger, J.-L., A. Diongue, A. Diedhiou, J. P. Ceron, M. Diop, J. F. Gueremy, and J. P. Lafore (2002), Multi-scale description of a Sahelian synoptic weather system representative of the West African monsoon, *Q. J. R. Meteorol. Soc.*, *128*, 1229–1257, doi:10.1256/003590002320373274.

Redelsperger, J.-L., C. Thorncroft, A. Diedhiou, T. Lebel, D. J. Parker, and J. Polcher (2006), African Monsoon Multidisciplinary Analysis (AMMA): An international research project and field campaign, *Bull. Am. Meteorol. Soc.*, *87*, 1739–1746, doi:10.1175/BAMS-87-12-1739.

Roca, R., J. Lafore, C. Piriou, and J. Redelsperger (2005), Extratropical dry-air intrusions into the West African Monsoon midtroposphere: An important factor for the convective activity over the Sahel, *J. Atmos. Sci.*, *62*, 390–407, doi:10.1175/JAS-3366.1.

Ross, R. J., and S. Rosenfeld (1997), Estimating mean weighted temperature of the atmosphere for Global Positioning System applications, *J. Geophys. Res.*, *102*, 21,719–21,730, doi:10.1029/97JD01808.

Saastamoinen, J. (1973), Contributions to the theory of atmospheric refraction, *Bull. Geod.*, *47*, 13–34, doi:10.1007/BF02522083.

Semazzi, F. H. M., and L. Sun (1997), The role of orography in determining the Sahelian climate, *Int. J. Climatol.*, *17*, 581–596, doi:10.1002/(SICI)1097-0088(199705)17:6<581::AID-JOC134>3.0.CO;2-E.

Singh, R. P., S. Dey, A. K. Sahoo, and M. Kafatos (2004), Retrieval of water vapor using SSM/I and its relation with the onset of monsoon, *Ann. Geophys.*, *22*, 3079–3083.

Sultan, B., and S. Janicot (2003), West African monsoon dynamics. Part II: The "pre-onset" and the "onset" of the summer monsoon, *J. Clim.*, *16*, 3407–3427, doi:10.1175/1520-0442(2003)016<3407:TWAMDP>2.0.CO;2.

Sultan, B., S. Janicot, and A. Diedhiou (2003), West African monsoon dynamics. Part I: Documentation of intraseasonal variability, *J. Clim.*, *16*, 3389–3406, doi:10.1175/1520-0442(2003)016<3389:TWAMDP>2.0.CO;2.

Takiguchi, H., T. Kato, H. Kobayashi, and T. Nakaegawa (2000), GPS observations in Thailand for hydrological applications, *Earth Planets Space*, *52*, 913–919.

Toledo Machado, L. A., J.-P. Duvel, and M. Desbois (1993), Diurnal variations and modulation by easterly waves of the size distribution of convective cloud clusters over West Africa and the Atlantic Ocean, *Mon. Weather Rev.*, *121*, 37–49, doi:10.1175/1520-0493.

Tregoning, P., and T. A. Herring (2006), Impact of a priori zenith hydrostatic delay errors on GPS estimates of station heights and zenith total delays, *Geophys. Res. Lett.*, *33*, L23303, doi:10.1029/2006GL027706.

Tregoning, P., and T. van Dam (2005), Atmospheric pressure loading corrections applied to GPS data at the observation level, *Geophys. Res. Lett.*, *32*, L22310, doi:10.1029/2005GL024104.

Walpersdorf, A., M.-N. Bouin, O. Bock, and E. Doerflinger (2007), Assessment of GPS data over Africa: Study of error sources and analysis of positioning accuracy, *J. Atmos. Sol. Terr. Phys.*, *69*, 1312–1330, doi:10.1016/j.jastp.2007.04.008.

Wang, J., and L. Zhang (2008), Systematic errors in global radiosonde precipitable water data from comparisons with ground-based GPS measurements, *J. Clim.*, *21*, 2218–2238, doi:10.1175/2007JCL11944.1.

Yang, G. Y., and J. Slingo (2001), The diurnal cycle in the tropics, *Mon. Weather Rev.*, *129*, 784–801, doi:10.1175/1520-0493(2001)129<0784:TDCITT>2.0.CO;2.

O. Bock, M. N. Bouin, and S. Nahmani, IGN, LAREG, ENSG-Cite Descartes, 6-8 avenue Blaise Pascal, Champs sur Marne, F-77455 Marne-la-Vallée CEDEX 2, France. (Olivier.Bock@ign.fr; Marie-Noelle.Bouin@meteo.fr; Samuel.Nahmani@ign.fr)

P. Collard and E. Doerflinger, Géosciences Montpellier, Université Montpellier II, UMR5243, CNRS, C.c. 060, Place E. Bataillon, F-34095 Montpellier CEDEX 05, France. (Philippe.Collard@dstu.univ-montp2.fr; erik@gm.univ-montp2.fr)

F. Didé, Direction Nationale de la Météorologie, BP 96, Cotonou, Benin. (dide_fral@yahoo.fr)

K. Gaptia Lawan Balawan, Direction de la Météorologie du Niger, BP 218, Niamey, Niger. (katielloulaw@yahoo.fr)

F. Guichard, GAME, URA1357, CNRS, 42, Avenue G. Coriolis, F-31057 Toulouse CEDEX, France. (francoise.guichard@meteo.fr)

S. Janicot, LOCEAN, Université Pierre et Marie Curie, UMR7159, CNRS, Boite 100, Couloir 45-55 4éme étage, 4 Place Jussieu, F-75252 Paris, France. (Serge.Janicot@locean-ipsl.upmc.fr)

M. Koité, Direction Nationale de la Météorologie, BP 237, Bamako, Mali. (mohasadio@yahoo.fr)

J. P. Lafore and M. Nuret, CNRM, Meteo-France, 42, Avenue G. Coriolis, F-31057 Toulouse CEDEX, France. (jean-philippe.lafore@meteo.fr; Mathieu.nuret@meteo.fr)

F. Masson, IPGS, Université Louis Pasteur, UMR7516, CNRS, 5 Rue René Descartes, F-67084 Strasbourg CEDEX, France. (Frederic.masson@eost.u-strasbg.fr)

R. Meynadier, Service d'Aéronomie, Université Pierre et Marie Curie, UMR7620, CNRS, Tour 45-46, 3e étage, Case 102, 4 Place Jussieu, F-75252 Paris CEDEX 05, France. (remi.meynadier@aero.jussieu.fr)

J.-B. Ngamini, ASECNA, BP 3144, Dakar, Senegal. (NGAMINIJEA@asecna.org)

D. Ouedraogo, ASECNA, BP 63, Ouagadougou 01, Burkina-Faso. (ohdidier@yahoo.fr)

S. Pokperlaar, Ghana Meteorological Agency, P.O. Box 9, Tamale, Ghana. (soami_pokperlaar@yahoo.com)